J Nonlinear Sci (2007) 17: 569–607
DOI 10.1007/s00332-007-9004-8

Journal of
Nonlinear
Science

A Numerical Study of the Stability of Solitary Waves of the Bona–Smith Family of Boussinesq Systems

V.A. Dougalis · A. Durán · M.A. López-Marcos · D.E. Mitsotakis

Received: 5 July 2006 / Accepted: 16 May 2007 / Published online: 28 July 2007

Abstract In this paper we study, from a numerical point of view, some aspects of stability of solitary-wave solutions of the Bona–Smith systems of equations. These systems are a family of Boussinesq-type equations and were originally proposed for modelling the two-way propagation of one-dimensional long waves of small amplitude in an open channel of water of constant depth. We study numerically the behavior of solitary waves of these systems under small and large perturbations with the aim of illuminating their long-time asymptotic stability properties and, in the case of large perturbations, examining, among other, phenomena of possible blow-up of the perturbed solutions in finite time.

Keywords Boussinesq systems · Stability of solitary waves

Mathematics Subject Classification (2000) 35Q53 · 65M60 · 76B25

Communicated by J. Bona.

V.A. Dougalis (✉) · D.E. Mitsotakis
Mathematics Department, University of Athens, 15784 Zographou, Greece
e-mail: doug@math.uoa.gr

V.A. Dougalis · D.E. Mitsotakis
Institute of Applied and Computational Mathematics, F.O.R.T.H., 71110 Heraklion, Greece

A. Durán · M.A. López-Marcos
Applied Mathematics Department, Faculty of Sciences, University of Valladolid, 47011 Valladolid, Spain

1 Introduction

We consider the Boussinesq systems of water wave theory, introduced in [8]:

$$\begin{aligned} &\eta_t + u_x + (\eta u)_x + a u_{xxx} - b\eta_{xxt} = 0, \\ &u_t + \eta_x + u u_x + c\eta_{xxx} - d u_{xxt} = 0, \end{aligned} \tag{1.1}$$

where $\eta = \eta(x,t)$ and $u = u(x,t)$ are real functions defined for $x \in \mathbb{R}$ and $t \geq 0$. The coefficients a, b, c, d are given by the formulas

$$\begin{aligned} a &= \frac{1}{2}\left(\theta^2 - \frac{1}{3}\right)\nu, \qquad & b &= \frac{1}{2}\left(\theta^2 - \frac{1}{3}\right)(1-\nu), \\ c &= \frac{1}{2}\left(1-\theta^2\right)\mu, \qquad & d &= \frac{1}{2}\left(1-\theta^2\right)(1-\mu), \end{aligned} \tag{1.2}$$

where ν and μ are real constants and $0 \leq \theta \leq 1$.

The family of systems (1.1) is an approximation of the two-dimensional Euler equations for the irrotational, free surface flow of an incompressible, inviscid fluid in a uniform horizontal channel, when the cross-channel variations can be ignored. The approximation is valid at appropriate time scales [8], when $\varepsilon := A/h \ll 1$, $\lambda/h \gg 1$, and the Stokes number $A\lambda^2/h^3$ is of order 1; here A is the maximum free surface elevation above an undisturbed level of fluid of depth h and λ is a typical wavelength. The derivation of (1.1) in [8] from the Euler equations leads to a system with dimensionless but scaled variables; this system is of the form (1.1), wherein the nonlinear terms $(\eta u)_x$ and uu_x, and the dispersive terms (the third-order derivatives) are multiplied by ε and the right-hand side consists of terms of order ε^2. Dropping the right-hand side terms yields systems for which the effects of nonlinearity and dispersion are comparable. In addition, unlike models incorporating one-way propagation assumptions, like the KdV and the BBM equations, the family of systems (1.1) describes two-way wave propagation.

In this paper we shall consider the systems in the form (1.1) wherein the variables are dimensionless but unscaled. The independent variables x and t are proportional to position along the channel and time, respectively, while the dependent variables $\eta(x,t)$ and $u(x,t)$ are proportional to the deviation of the free surface from its undisturbed level at (x,t) and to the horizontal velocity of the fluid at (x,t) at a nondimensional height $y = -1 + \theta(1+\eta(x,t))$, respectively. (In terms of the variable y, the flat bottom of the channel lies at $y = -1$.) For the details of the derivation of systems of this type and of related equations, cf. [8, 15, 33, 43].

The *Bona–Smith* family of systems, introduced in [13], are Boussinesq systems of the form (1.1, 1.2) obtained by requiring that $\nu = 0$ and $b = d$. The latter condition yields that $\mu = (4 - 6\theta^2)/3(1-\theta^2)$ for $\theta \neq 1$, and, as a consequence, the constants of the Bona–Smith systems are given by the formulas

$$a = 0, \qquad b = d = \frac{3\theta^2 - 1}{6}, \qquad c = \frac{2 - 3\theta^2}{3}. \tag{1.3}$$

We shall also consider the system obtained by setting $\theta = 1$ in (1.3), i.e. the system with parameters $a = 0$, $b = d = 1/3$, $c = -1/3$, which, although not properly of the

form (1.1, 1.2), may be considered nevertheless as a limiting case in the limit $b = d$ and $\mu \to -\infty$. We refer the reader to the remarks in [13] and [8] as to the order of magnitude of the terms of this limit system when written in scaled variables and considered as approximation to the Euler equations. We also remark that setting $\theta^2 = 2/3$ in (1.3) yields the BBM–BBM system corresponding to $a = c = 0$, $b = d = 1/6$; this system was analyzed in [7].

If we consider the linearized system that we obtain from (1.1, 1.3) by dropping the nonlinear terms, and seek solutions of the form $e^{i(kx-\omega t)}$, we see that the dispersion relation for the Bona–Smith systems is

$$\omega^2 = \frac{k^2(1-ck^2)}{(1+bk^2)^2}, \quad \text{with } \omega'(k) = \pm\frac{1-(b+2c)k^2}{\sqrt{1-ck^2}(1+bk^2)^2}.$$

From these formulas it follows that, as $k \to \pm\infty$, the frequency approaches a constant while the phase velocity ωk^{-1} and the group velocity $\omega'(k)$ tend to zero. Hence, as was already observed in [13], large wave components simply lead to standing oscillations of finite frequency, which is a first indication that (1.1, 1.3) has favorable properties as a system modelling the Euler equations. Indeed, it follows from the analysis in [8] that the initial-value problem for the linearized system corresponding to (1.1, 1.3) is well posed in $H^{s+1} \times H^s$ for $s \geq 0$ if $\theta^2 > 2/3$ and in $H^s \times H^s$ if $\theta^2 = 2/3$ (here $H^s = H^s(\mathbb{R})$ is the usual, L^2-based Sobolev space of functions on $\mathbb{R}$) and conserves "energy" in the sense explained in Sect. 3 of [8]. (The systems are linearly ill posed if $\theta^2 < 2/3$; hence, we restrict ourselves to the parameter range $2/3 \leq \theta^2 \leq 1$ in the sequel.) It also follows from [8] that for $\theta^2 \in (2/3, 1]$ the linearized system is well posed in the L^p-based Sobolev spaces $W_p^{s+1} \times W_p^s$ for all $s \geq 0$ and $p \in (1, \infty)$, while it is ill posed for $p = 1$ or ∞. The BBM–BBM system with $\theta^2 = 2/3$ is well posed in L^p for $1 \leq p \leq \infty$ in the sense explained in [8].

We turn now to the Cauchy problem for the nonlinear Bona–Smith system, i.e. to determining the solution of the system

$$\begin{aligned} &\eta_t + u_x + (\eta u)_x - b\eta_{xxt} = 0, \\ &u_t + \eta_x + uu_x + c\eta_{xxx} - bu_{xxt} = 0, \\ &\quad b = \frac{3\theta^2-1}{6}, \quad c = \frac{2-3\theta^2}{3}, \quad \frac{2}{3} \leq \theta^2 \leq 1, \end{aligned} \tag{1.4}$$

for $x \in \mathbb{R}$, $t > 0$, with initial conditions

$$\eta(x,0) = \eta_0(x), \qquad u(x,0) = u_0(x), \tag{1.5}$$

where η_0 and u_0 are given functions on $\mathbb{R}$. The initial-value problem (1.4, 1.5) has been studied in detail by Bona and Smith [13] in the case $\theta^2 = 1$. A straightforward extension of their theory (see also [9]) yields that if the initial data (1.5) are such that $\eta_0 \in H^1 \cap C_b^3$ and $u_0 \in L^2 \cap C_b^2$ (where $C_b^k = C_b^k(\mathbb{R})$ denotes the space of bounded, continuous functions on $\mathbb{R}$ whose first k derivatives are also continuous and bounded) and if $\eta_0(x) > -1$ for $x \in \mathbb{R}$ and

$$E(0) := \int_{-\infty}^{\infty} \left[\eta_0^2 + |c|\left(\eta_0'\right)^2 + (1+\eta_0)u_0^2\right] \mathrm{d}x < 2|c|^{1/2}, \tag{1.6}$$

then there is a unique, global classical solution (η, u) of the initial-value problem (1.4, 1.5), which, for each $T > 0$, is a continuous map from $[0, T]$ into $(H^1 \cap C_b^3) \times (L^2 \times C_b^2)$. If further regularity is assumed for the initial data, then (1.4, 1.5) may be shown to be well posed in $H^{s+1} \times H^s$ for $s \geq 0$ or in $(H^1 \cap C_b^{s+1}) \times (L^2 \cap C_b^s)$ for integer $s \geq 0$.

As explained in [13], the crucial step in the proof of global well-posedness of the Bona–Smith systems is establishing an a priori $H^1 \times L^2$ estimate of the solution. This estimate follows from the fact that the system is Hamiltonian and the "energy" functional,

$$E(t) := \int_{-\infty}^{\infty} \left[\eta^2 + |c|\eta_x^2 + (1+\eta)u^2\right] \mathrm{d}x, \tag{1.7}$$

remains invariant for $t \geq 0$. The restrictions $\theta^2 > 2/3$ and $\eta_0 > -1$ ensure that $1 + \eta(x, t)$, and, consequently, $E(t)$ remain positive for all $x \in \mathbb{R}$ and $t \geq 0$. (Recall that $1 + \eta(x, t) > 0$ means that there is water in the channel at the point x at time t.) If $\theta^2 = 2/3$, the system (1.4) reduces to the BBM–BBM system, which may be shown to be well posed in $H^s \times H^s$ for $s \geq 0$, locally in time; cf. [7, 9].

For the purposes of solving numerically the system (1.4) and/or comparing its solution with experimental data, it is important to establish well-posedness, at least locally in time, of *initial- and boundary-value problems* for (1.4). For the *periodic* initial-value problem (1.4, 1.5), $\theta^2 > 2/3$, on the spatial interval $[-L, L]$, $L > 0$, it was shown in [2] (see also [4]) that if, for example, $(\eta_0, u_0) \in C_\pi^3(-L, L) \times C_\pi^2(-L, L)$ (where $C_\pi^k(-L, L)$ for integer $k \geq 0$ are the k times continuously differentiable periodic functions on $[-L, L]$), $\eta_0 > -1$ and

$$\int_{-L}^{L} \left[\eta_0^2 + |c|\left(\eta_0'\right)^2 + (1+\eta_0)u_0^2\right] \mathrm{d}x < \frac{2L|c|^{1/2}}{L + |c|^{1/2}}, \tag{1.8}$$

then there is a unique, global classical solution (η, u) of the periodic initial-value problem for (1.4, 1.5), which, for each $T > 0$, is a continuous map from $[0, T]$ into $C_\pi^3(-L, L) \times C_\pi^2(-L, L)$. In this case too it is easy to check that the energy functional, defined now as

$$E(t) := \int_{-L}^{L} \left[\eta^2 + |c|\eta_x^2 + (1+\eta)u^2\right] \mathrm{d}x, \tag{1.9}$$

is constant in t. (Note that the bound in the right-hand side of (1.8) tends, as $L \to \infty$, to the right-hand side $2|c|^{1/2}$ of the analogous inequality for the problem on the whole real line.)

Other types of boundary conditions may also be shown to lead to well-posed initial- and boundary-value problems for the Bona–Smith systems, cf. [2, 4]. For example, the problem with the *reflection* boundary conditions $\eta_x = 0$ and $u = 0$ imposed at both endpoints $x = \pm L$ is globally well-posed if $\theta^2 > 2/3$; the energy E, given by (1.9), is conserved in this case. Imposing $\eta = 0$, $u = 0$ at the endpoints leads to a problem for which $E(t)$ is not constant and for which one may prove existence and uniqueness of smooth solutions only locally in time.

Being approximations of the Euler equations, the Boussinesq systems may be reasonably expected to possess *solitary-wave* solutions. To study such solutions for the Bona–Smith system, we seek travelling-wave solutions of (1.4) of the form

$$\begin{aligned} &\eta_s(x,t) = \eta_s(x + x_0 - c_s t), \\ &u_s(x,t) = u_s(x + x_0 - c_s t), \quad x, x_0 \in \mathbb{R},\ t \geq 0, \end{aligned} \tag{1.10}$$

where c_s is the (constant) speed of propagation of the wave. The univariate functions $\eta_s = \eta_s(\xi)$, $u_s = u_s(\xi)$, $\xi \in \mathbb{R}$, will be supposed to be smooth, positive, and even, with a single maximum located at $\xi = 0$, and decaying monotonically to zero, along with all their derivatives, as $\xi \to \pm\infty$. Substituting the formulas (1.10) into (1.4), integrating once and denoting $(u_s(\xi), \eta_s(\xi))$ simply by $(u(\xi), \eta(\xi))$ yields a system of two nonlinear ordinary differential equations (o.d.e.) which is written (with the notation of [18])

$$S_1 \mathbf{y}'' + S_2 \mathbf{y} + \nabla g(u,\eta) = 0, \quad \xi \in \mathbb{R}, \tag{1.11}$$

where $\mathbf{y} = (u,\eta)^{\mathrm{T}}$, $' = \frac{\mathrm{d}}{\mathrm{d}\xi}$, and

$$S_1 = -6\begin{pmatrix} 0 & b \\ b & \frac{c}{c_s} \end{pmatrix}, \qquad S_2 = -\frac{6}{c_s}\begin{pmatrix} 1 & -c_s \\ -c_s & 1 \end{pmatrix}, \qquad g(u,\eta) = -\frac{3}{c_s}u^2\eta. \tag{1.12}$$

Note that if $(u,\eta)^{\mathrm{T}}$ is a solution of (1.11) corresponding to some $c_s > 0$, then $(-u,\eta)^{\mathrm{T}}$ is also a solution that propagates with speed $-c_s$, i.e. to the left as t increases. Henceforth, we shall normally assume that c_s is positive.

Existence of solutions of the o.d.e. system (1.11, 1.12) in the case of the Bona–Smith system with $\theta^2 = 1$ was established, for any $c_s > 1$, by Toland [37]. Subsequently Toland showed in [39], by a geometric proof, that more general similar o.d.e. systems possess, under certain hypotheses, symmetric orbits that are homoclinic to zero. Toland's general theory was applied by Chen [18] to establish the existence of solitary-wave solutions for several examples of Boussinesq systems, including the BBM–BBM system, corresponding to the special case of (1.11, 1.12) with $\theta^2 = 2/3$.

It is not hard to check, cf. [19], that Toland's theory can also be applied to establish the existence of solitary waves for any value of the speed $c_s > 1$ for all Bona–Smith systems, i.e. for any $\theta^2 \in [2/3, 1]$. It also follows from this theory that for a solitary wave the pair of peaks $(u(0), \eta(0))$ must lie in the open segment $\Gamma = P_1P_2$ (which does not include the origin) of the branch of the curve $f(u,\eta) = 0$ in the first quadrant of the u,η-plane (cf. Fig. 1), where $f(u,\eta) := \mathbf{y}^{\mathrm{T}} S_2 \mathbf{y} + 2g(u,\eta)$, i.e. where

$$f(u,\eta) = \frac{6}{c_s}\big(-u^2(1+\eta) - \eta^2 + 2c_s u\eta\big). \tag{1.13}$$

It follows that the speed c_s of a solitary wave with peaks $(u(0), \eta(0))$ satisfies the equation

$$c_s = \frac{\mu^2(1+\eta(0)) + 1}{2\mu}, \quad \mu = \frac{u(0)}{\eta(0)}. \tag{1.14}$$

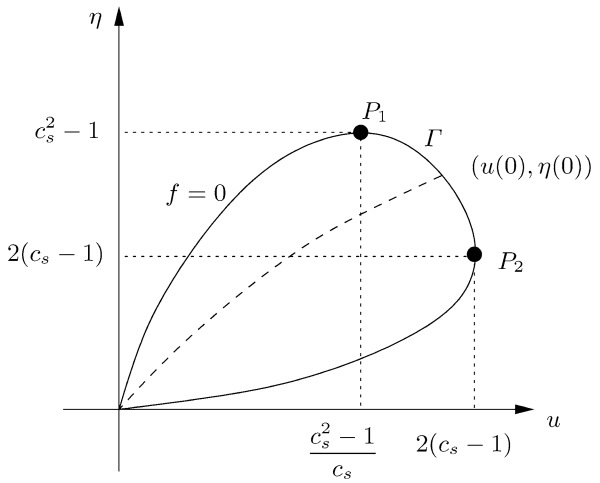

Fig. 1 Locus of possible $(u(0), \eta(0))$ and orbits

The curve $f = 0$ and, consequently, the relation (1.14) does not explicitly involve the coefficients of the dispersive terms of the Boussinesq system. In particular, (1.14) must hold for any triplet $(c_s, u(0), \eta(0))$ corresponding to a solitary wave of a Bona–Smith system. Of course, given any value of $c_s > 1$, the location of the point $(u(0), \eta(0))$ on Γ and the shape of the corresponding solitary-wave profile (i.e. the orbit $(u(\xi), \eta(\xi))$, $0 \le \xi < \infty$, represented by a dashed line in Fig. 1) depends on θ^2. Note that it follows from Toland's theory that $\eta(0) > u(0)$. In addition, it is easily seen from (1.14) that $\frac{\partial c_s}{\partial \eta(0)} > 0$, $\frac{\partial c_s}{\partial u(0)} > 0$, implying that the speed of solitary waves increases with their height.

The question of *uniqueness* of these solitary waves may be studied by techniques again due to Toland, who established uniqueness in the case of the $\theta^2 = 1$ system, unconditionally if $u(0) \le 1$, and in general, provided $1 < c_s \le 3/2$ or $c_s \gg 1$, cf. [38]. In the case of a general Bona–Smith system it is possible, following the general line of Toland's proof, to show uniqueness of solitary waves if

$$\theta^2 \in \left(\frac{2+\sqrt{0.2}}{3}, 1\right] \quad \text{and}$$

$$1 < c_s \le c_{s,\max}(\theta) := \min\left\{\frac{12(3\theta^2-2)}{21\theta^2-13}, \frac{2(3\theta^2-2)}{\sqrt{3(1-\theta^2)(3\theta^2-1)}}\right\};$$

see [19]. This result means that (at least) for the class of Bona–Smith systems corresponding to $\theta^2 \in (\frac{2+\sqrt{0.2}}{3}, 1]$, and given any value of the speed in the interval $(1, c_{s,\max}(\theta)]$, there exists precisely one point $(u(0), \eta(0)) \in \Gamma$, i.e. one pair $(u(0), \eta(0))$ satisfying (1.14), from which there issues a solitary wave of the corresponding system. This solitary wave is represented by the solution of the initial-value problem for (1.11, 1.12) with initial conditions $u(0)$, $\eta(0)$, $u'(0) = 0$, $\eta'(0) = 0$.

Some solitary-wave solutions of the Bona–Smith systems can be found in closed form. Following, e.g. [17], we assume that

$$\begin{aligned} \eta_s(x,t) &= \eta_0 \operatorname{sech}^2\big(\lambda(x+x_0-c_s t)\big), \\ u_s(x,t) &= B\eta_s(x,t), \end{aligned} \tag{1.15}$$

where η_0, B, λ are real constants and x_0 is arbitrary. When these formulas are substituted in the o.d.e. system (1.11, 1.12), it transpires that for each value of θ^2 in the interval $(7/9, 1)$ there is precisely one solitary-wave solution (η_s, u_s) of the form (1.15); the parameters η_0, c_s, B, λ are given in terms of θ^2 by the formulas

$$\begin{aligned} \eta_0 &= \frac{9}{2}\cdot\frac{\theta^2-7/9}{1-\theta^2}, \qquad c_s = \frac{4(\theta^2-2/3)}{\sqrt{2(1-\theta^2)(\theta^2-1/3)}}, \\ \lambda &= \frac{1}{2}\sqrt{\frac{3(\theta^2-7/9)}{(\theta^2-1/3)(\theta^2-2/3)}}, \qquad B = \sqrt{\frac{2(1-\theta^2)}{\theta^2-1/3}}. \end{aligned} \tag{1.16}$$

It should be stressed that for each $\theta^2 \in (7/9, 1)$, the corresponding system of the Bona–Smith family possesses only one exact solitary-wave solution of the form (1.15); its corresponding parameters and, in particular, its speed are given by the formulas (1.16). Of course, from the existence theory previously outlined, it is known that for each $\theta^2 \in [2/3, 1]$ and for *any* value of the speed $c_s > 1$, there exists a solitary wave of the corresponding system; this solitary wave has the property that $(u(0), \eta(0)) \in \Gamma$ so that (1.14) is satisfied.

Solitary waves are not just interesting special travelling-wave solutions of nonlinear dispersive wave equations; their importance lies in the distinguished role they play in the evolution and long-time asymptotic behavior of general solutions of the initial-value problem for these equations, which emanate from arbitrary initial data in appropriate function classes. *Resolution* of initial data into a series of solitary waves plus decaying, small, dispersive oscillatory tails has been rigorously proved, via the inverse scattering transform, for integrable equations such as the KdV equation, cf. e.g. [35], and has, of course, been observed numerically since the re-emergence of the study of solitary waves [45] in the 1960s in the case of many integrable and nonintegrable systems. For some recent relevant numerical studies, cf. e.g. [10, 11, 20, 32], and in particular for Boussinesq systems, e.g. [2–4, 7, 31].

Related to the resolution property, and almost a prerequisite for it, is the stability of solitary waves under small perturbations. The rigorous theory of *orbital* (or *shape*) *stability* of solitary waves of the KdV and the BBM equations was initiated by Benjamin [5] (see also [6]), who established stability by Liapunov's direct method. In this *variational theory* the solitary wave is characterized as an extremal of an invariant of the equation under the constraint that a second conserved functional is held fixed. Specifically, in [5] the solitary wave is characterized as an extremum of the "moment of instability", which happens to be the Hamiltonian of the underlying partial differential equation (p.d.e.), while the second conserved functional is the square of the L^2 norm, respectively, of the H^1 norm, of the solution of the KdV, respectively, of the BBM equation. The velocity of the solitary wave is the Lagrange multiplier

of this constrained variational problem. This classical method, whose origins can be traced again to Boussinesq [16], was extended, improved, and applied to establish the orbital stability (or instability) of solitary waves of a variety of nonlinear dispersive wave equations by many authors, for example Weinstein [40, 41], Grillakis et al. [22], Albert et al. [1], Bona et al. [14], and others. A basic ingredient of this theory is the spectral analysis of some linear ordinary differential operators on the real line with coefficients that depend on the profiles of the solitary waves of the specific equation.

In the case at hand, the application of this orbital stability theory would proceed as follows. As it was mentioned earlier, the Bona–Smith system (1.4) is Hamiltonian [9]. Indeed, recalling the definition of the invariant E from (1.7), we see that the functional

$$H := -\frac{1}{2}E = \frac{1}{2}\int_{-\infty}^{\infty}\left[c\eta_x^2 - \eta^2 - (1+\eta)u^2\right]\mathrm{d}x \tag{1.17}$$

is a Hamiltonian, since the system (1.4) may be written in the form

$$\partial_t \begin{pmatrix}\eta\\ u\end{pmatrix} = J\delta H\begin{pmatrix}\eta\\ u\end{pmatrix}, \tag{1.18}$$

where J is the antisymmetric operator $(1-b\partial_x^2)^{-1}\partial_x\left(\begin{smallmatrix}0&1\\1&0\end{smallmatrix}\right)$ and the gradient δH is computed with respect to the $L^2\times L^2$ inner product. The phase space may be defined as a suitable product of Sobolev classes with elements vanishing at infinity along with an appropriate number of their derivatives. In addition, solutions of the system (1.4) preserve the impulse functional

$$I := \int_{-\infty}^{\infty}(u\eta + bu_x\eta_x)\,\mathrm{d}x. \tag{1.19}$$

The variational theory characterizes the solitary waves (η_s, u_s), (1.10) as extremals of H for fixed I. This means that the solitary waves are critical points of the functional $G(\eta, u)$, where

$$G := H - c_s I.$$

The theory requires further to compute the Hessian $G'' = H'' - c_s I''$ evaluated at the solitary wave (η_s, u_s) and check that it has a simple zero eigenvalue, at most a finite number of negative eigenvalues, with the rest of spectrum positive and bounded away from zero. In our case we find that

$$S := G''(\eta_s, u_s) = \begin{pmatrix} -(1+c\partial_x^2) & c_s(1-b\partial_x^2) - u_s\\ c_s(1-b\partial_x^2) - u_s & -(1+\eta_s)\end{pmatrix}.$$

We may thus write that $S = S_\infty + A$, where

$$S_\infty := \begin{pmatrix} -(1+c\partial_x^2) & c_s(1-b\partial_x^2)\\ c_s(1-b\partial_x^2) & -1\end{pmatrix}, \qquad A := \begin{pmatrix} 0 & -u_s\\ -u_s & -\eta_s\end{pmatrix}.$$

Since η_s, $u_s \to 0$ exponentially as $|x|\to\infty$, A is relatively compact. Therefore, by Weyl's theorem [23, 34], the essential spectrum of S coincides with that of S_∞.

For the constant coefficient operator S_∞, using Fourier analysis we readily find that the essential spectrum is the union of the intervals $(-\infty, -(1+c_s)]$, $[-1+c_s, \infty)$. Hence, there is an infinite number of directions in which G'' is indefinite and the variational theory cannot be applied. This is a typical way of failure of the classical theory, also observed in the case of various other nonlinear dispersive equations and systems, cf. e.g. [12, 24, 27, 29, 36].

Orbital stability implies that an initial profile $w(x,0)$, which is a small perturbation of a solitary wave $w_s(x)$, will evolve into a solution $w(x,t)$, which, for all t, will remain close to the family of translated profiles $w_s(x+\xi)$, $\xi \in \mathbb{R}$. More detailed information about the long-time asymptotic behavior of $w(x,t)$ may be furnished by studies of the *asymptotic stability* of solitary waves. Such studies have been carried out in the case of one-way models such as the KdV and BBM equations and their generalized variants, e.g. in [26, 28, 42] and assert, grosso modo, that for large t,

$$w(x,t) = w_{s_\infty}(x - c_\infty t + \xi_\infty) + z(x,t),$$

where w_{s_∞} is a solitary wave with speed c_∞ close to the speed c_s of the originally perturbed w_s, and ξ_∞ is a small phase shift. The part of w denoted by $z(x,t)$ represents smaller (and slower) solitary waves that may have also been produced, as well as the small amplitude, dispersive, oscillatory tail trailing the solitary waves. Hence, $z(x,t)$ appears to be convected to the left relative to the larger emerging solitary wave w_{s_∞} and the aim of the theory of asymptotic stability of solitary waves is to show that z tends to zero as $t \to \infty$ in an appropriate sense ("convective stability"). For more recent studies of asymptotic stability of solitary waves for these equations, cf. [25] and [21]. Many of these studies include estimates of the decay of solutions of the nonlinear equations satisfied by z, as well as estimates of how the speed and phase of the main pulse approach c_∞ and ξ_∞, respectively, as $t \to \infty$. Pego and Weinstein in [29] have analyzed the *linearized* convective stability of solitary waves for the fourth-order (regularized) Boussinesq equation $w_{tt} = w_{xx} + \frac{3}{2}(w^2)_{xx} + \frac{1}{3}w_{xxtt}$ and the "classical" Boussinesq system (cf. [43]; this system corresponds to the values $a = b = c = 0$, $d = \frac{1}{3}$ in (1.1)). The term "linearized" refers to the fact that the equation (or system) for the residual z analyzed in [29] is not the exact nonlinear equation that z satisfies but is obtained by linearizing this equation in a frame of reference moving with the speed of the original unperturbed solitary wave. A similar study in the case of the Bona–Smith systems is currently underway by the authors of the present paper.

In view of the difficulties in establishing an exact nonlinear theory for orbital or asymptotic stability for the Boussinesq systems, we carry out in this paper a numerical study of various stability properties of the solitary waves of the Bona–Smith family (1.4). We approximated solutions of the Cauchy problem of (1.4) by solving numerically the periodic initial-value problem for large-enough periods $2L$. The main numerical scheme that we used was a fully discrete Galerkin-finite element method based on cubic spline discretizations on a uniform mesh on $[-L, L]$, and the classical, explicit fourth-order Runge–Kutta scheme for the time-stepping procedure. This scheme has been analyzed in [2, 4] and proved to be numerically stable and of fourth order of accuracy in space and time; it is outlined here in Appendix 1. (Other numerical schemes that have been analyzed and used for the Bona–Smith system include a

semidiscrete, nonstandard Galerkin method due to Winther [44], and a fully discrete spectral method [30, 31].)

In the paper at hand we make a numerical study of the effect of perturbations on solitary-wave solutions of (1.4). In Sect. 2 we study the effect of small perturbations. Our numerical experiments suggest that the solitary waves are asymptotically stable. We examine in detail the small amplitude dispersive tails that emerge (and travel in both directions) in addition to the main solitary waves. In Sect. 3 we consider some effects of larger perturbations of initial solitary-wave profiles. These include the generation of many solitary waves travelling in both directions, when the initial perturbation is large enough. We also briefly look at the interactions between colliding solitary waves; for more computations along this line cf. [2, 4]. In some cases, we observe that suitable large initial disturbances lead to apparent blow-up of the solution in finite time and present evidence to the effect that the condition $1+\eta(x,t)<0$, at some point x at some time instant $t>0$, is necessary but not sufficient for the development of singularities in the solution. With the exception of this type of violent instability due to large, nonphysical initial perturbations, the solitary waves of the system (1.4) appear to be stable under a variety of types of perturbations. In Appendix 1 we present in detail the numerical scheme that we used to perform the numerical experiments of Sects. 2 and 3 and review its stability and accuracy theory. We also study in detail the accuracy of two procedures that we used to generate solitary waves numerically, cutting them away from the rest of the solution. In Appendix 2 we list the types of perturbations of solitary waves that we used along with tables of the parameters (amplitude, speed, etc.) of the larger solitary waves that emerge. In Appendix 3 we summarize the parameters $\eta_{\max}, u_{\max}, c_s$ of the emerging solitary waves in a figure in the u,η-plane, which suggests that for a given θ^2, i.e. a given member of the Bona–Smith family of systems, the peak point $(u_{\max},\eta_{\max})$ of the solitary wave is a smooth, univalent function of c_s. (In Sect. 2 we remark that $u_{\max}$, $\eta_{\max}$ increase with c_s.)

2 Effect of Small Perturbations: Numerical Study of Asymptotic Stability

In the numerical experiments to be described in this section, initial profiles representing exact or numerically generated solitary waves of the Bona–Smith system were subjected to small perturbations of several kinds. In all cases the perturbed initial wave resolved itself, relatively fast, into a "nearby" solitary wave plus a two-way propagating dispersive oscillatory tail. As the magnitude of the perturbations grew, one or more smaller solitary waves were generated as well; these waves travelled to the right or the left. In this section, we present a synopsis of our numerical investigations of these *asymptotic stability* properties of the solitary waves. We mostly concentrate on small perturbation cases, wherein typically one solitary wave, and in some cases two, emerge, and describe the evolution up to the establishment of these waves and the development of the dispersive tail. The study of the formation of more solitary waves and of other effects of larger perturbations is postponed until Sect. 3.

2.1 Evolution of a Slightly Perturbed Solitary Wave

We begin by describing a typical experiment. We start from an initial condition of the form (1.15, 1.16) at $t = 0$ and perturb the amplitude of $\eta_s(x, 0)$ by a factor $r > 0$. Specifically, we integrate (1.4, 1.5) with $\theta^2 = 9/11$, taking

$$\begin{aligned} \eta_0(x) &= r\eta_0 \operatorname{sech}^2\big(\lambda(x + x_0)\big), \\ u_0(x) &= B\eta_0 \operatorname{sech}^2\big(\lambda(x + x_0)\big), \end{aligned} \tag{2.1}$$

where $\eta_0 = 1$, $B = \sqrt{3}/2$, $\lambda = \frac{1}{4}\sqrt{\frac{33}{5}}$, $x_0 = 100$. (The unperturbed solitary wave would have travelled to the right with speed $c_s = 5\sqrt{3}/6 \cong 1.443376$.) We solved numerically the system for various values of r up to $t = 100$. (Unless otherwise specified, in the numerical simulations we integrated on the spatial interval $[-150, 150]$ with $h = 0.1$ and $k = 0.01$.) A typical temporal evolution, corresponding to $r = 1.1$, is depicted in Fig. 2, which shows the sequence of the numerically computed η and u profiles as functions of x at $t = 0, 40, 100$. The initially perturbed solitary wave resolves itself into a single solitary wave with $\eta_{\max} \cong 1.06110$, $u_{\max} \cong 0.91152$, travelling to the right with speed $c_s \cong 1.4673$, and followed by a small-amplitude dispersive oscillatory tail. Another dispersive oscillatory wavetrain, of slightly larger amplitude propagates to the left and, by $t = 100$, has wrapped itself around the boundary due to the periodic boundary conditions.

Associated with this computation are the short-time temporal evolution curves of the amplitudes and speed of the η and u solitary waves, shown in Fig. 3. The speed refers to the velocity of the point $x^*(t)$ at which the pulse attains its maximum (cf. Appendix 1 for comments on computing x^* and other parameters of solitary waves. Due to the short time-span of the initial stage of this evolution, we computed the velocity of x^* as $(x^*(t) - x^*(t + \Delta t))/\Delta t$, taking $\Delta t = 0.2$ instead of the value $\Delta t = 10$ normally used in steady-state speed calculations.) After an initial, transient phase the amplitudes and the speed are seen to settle to their steady-state values that correspond to the parameters $\eta_{\max}$, $u_{\max}$, c_s of the emerging solitary wave.

As the perturbation factor r grows, more solitary waves emerge. For example, after about $r = 1.6$, and definitely by $r = 1.8$, as seen in Fig. 17 of Appendix 1, in addition to the main, rightward-travelling solitary wave, a second, smaller solitary wave emerges quite early at the head of the leftward-travelling wavetrain. For larger values of r we observe more solitary waves travelling in either direction; the parameters of the largest solitary wave and the number of solitary waves that have appeared up to $t = 100$ are shown in Table 10 of Appendix 2.

In Appendix 2 we also summarize the results of other numerical experiments that we performed using various types of perturbations of initial solitary wave profiles, mainly on the system with $\theta^2 = 9/11$. If the magnitude of the perturbation was small, we observed in all cases a typical evolution having the same characteristics as the one resulting from the perturbation of the amplitude of $\eta_0(x)$ that we just described. We also performed similar experiments by perturbing by small amounts in various directions in the function space solitary waves of other Bona–Smith systems, and in particular of those corresponding to the limiting cases $\theta^2 = 1$ (the "classical" system)

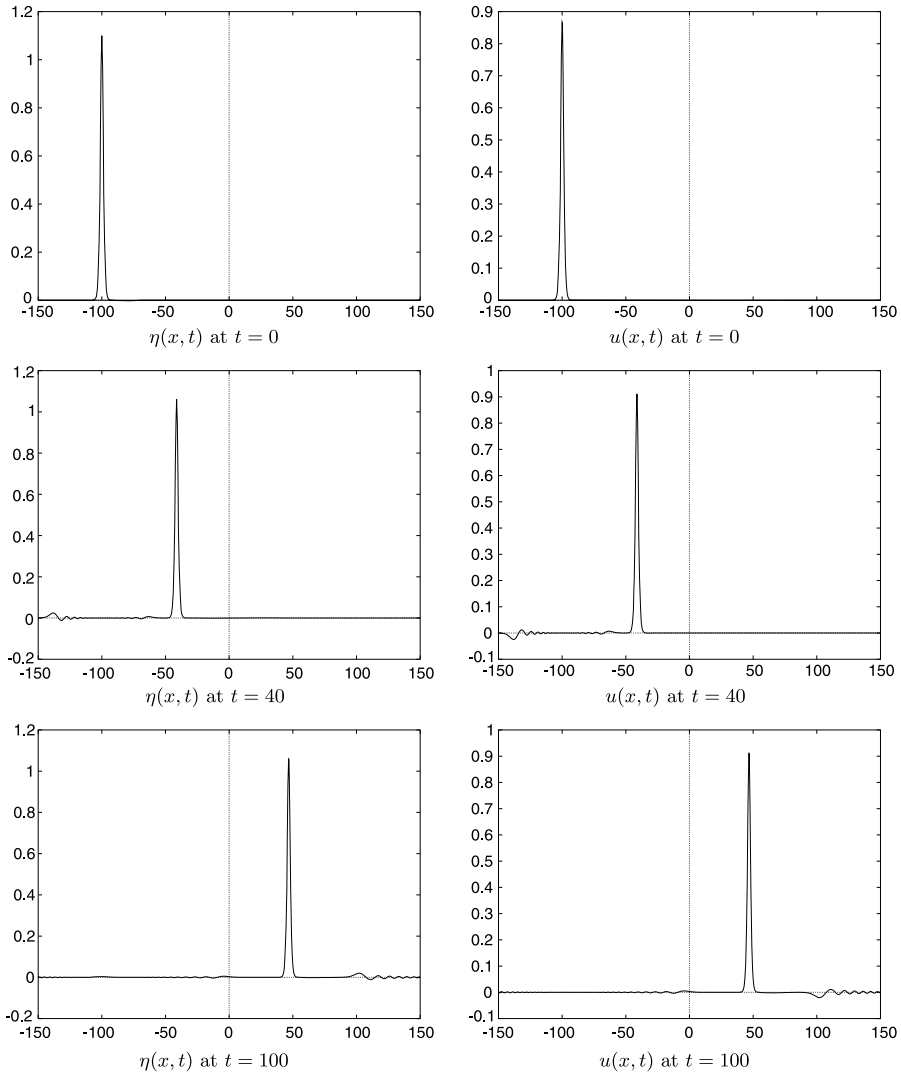

Fig. 2 Evolution of a perturbed solitary wave, $\theta^2 = 9/11$. Initial conditions (2.1), $r = 1.1$

and $\theta^2 = 2/3$ (the BBM–BBM system). For many of these systems (in particular for the $\theta^2 = 1$ and $\theta^2 = 2/3$ cases), we recall that there exist no analytical formulas for the solitary waves; so, the initial profiles of the solitary waves were constructed by iterative cleaning (cf. Appendix 1). We also obtained the same behavior when we integrated a fixed initial solitary wave under small perturbations of the coefficients of the dispersive terms of the system, as in Case IV in Appendix 2.

The numerical experiments mentioned above suggest that the solitary waves of the Bona–Smith systems are *asymptotically stable* under small perturbations in the sense explained in the Introduction. Indeed, what is observed is that an initial solitary wave,

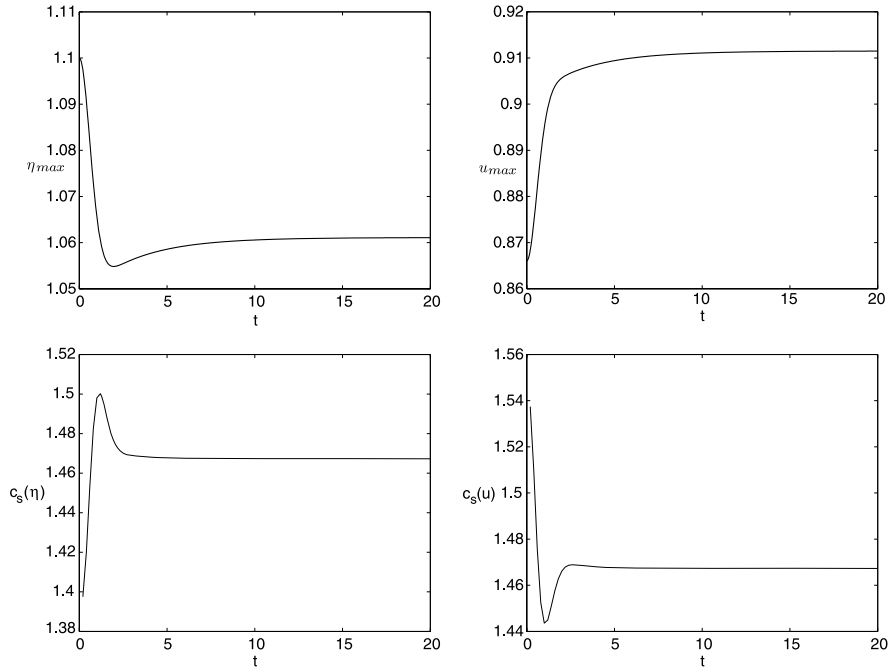

Fig. 3 Initial stage of the evolution of the amplitude and speed of the emerging solitary wave, $\theta^2 = 9/11$. Initial conditions (2.1), $r = 1.1$

when perturbed by a small amount, forms a dominant solitary wave (main pulse) that is followed by dispersive tails travelling in both directions and possibly by smaller solitary waves also travelling in both directions. The main pulse outruns the smaller waves and tends, as time grows, to a solitary wave with parameters close to those of the original, unperturbed solitary wave.

2.2 Dependence of $\eta_{\max}$, $u_{\max}$ on c_s

Assuming *uniqueness* of solitary waves, in the sense explained in the Introduction, we conclude that given a value of $c_s > 1$ there is a unique pair of peak values $(\eta(0), u(0)) = (\eta_{\max}, u_{\max})$ of the corresponding solitary wave. In all numerical experiments that we performed, using various types of perturbations of initial solitary wave profiles, we have consistently observed that $\eta(0)$ and $u(0)$ appear to be smooth, increasing functions of c_s, so that larger solitary waves outrun smaller ones. (We have already mentioned in the Introduction that formula (1.14) implies that $\frac{\partial c_s}{\eta(0)} > 0$ and $\frac{\partial c_s}{u(0)} > 0$.) For example, consider Table 10 in Appendix 2, which gives the numerically computed peak values $\widetilde{\eta}_{\max}$, $\widetilde{u}_{\max}$ and their associated speeds $\widetilde{c}_s$ in the case of the Bona–Smith system with $\theta^2 = 9/11$ and perturbations of the type (5.1). (When substituted in (1.14), these values of $\widetilde{\eta}_{\max}$, $\widetilde{u}_{\max}$ yield a speed c_s that differs from $\widetilde{c}_s$ by an amount of $O(10^{-6})$.) Plotting $\widetilde{\eta}_{\max}$ and $\widetilde{u}_{\max}$ as functions of $\widetilde{c}_s$ using the data of Table 10 yields Fig. 4 in which $\widetilde{\eta}_{\max}$ and $\widetilde{u}_{\max}$ appear to be smooth, increasing functions of $\widetilde{c}_s$.

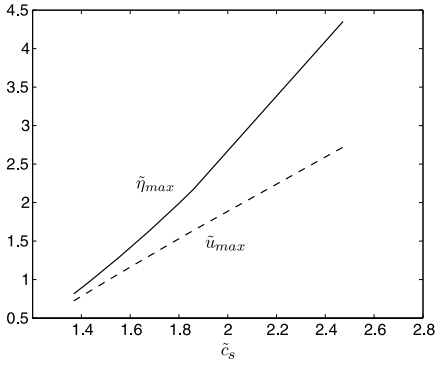

Fig. 4 Peak values of the numerical solitary waves as functions of the speed. Data of Table 10

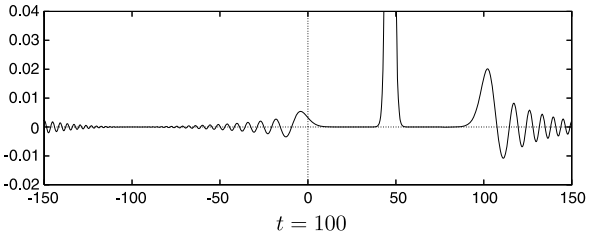

Fig. 5 Dispersive tails of η. (Magnification of the η-profile at $t = 100$, Fig. 2)

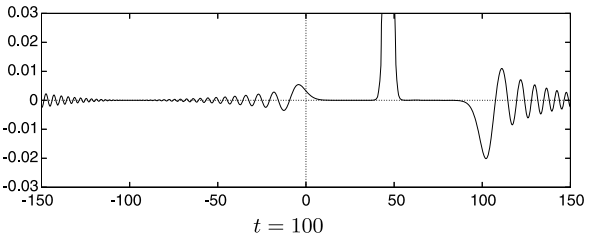

Fig. 6 Dispersive tails of u. (Magnification of the u-profile at $t = 100$, Fig. 2)

2.3 Numerical Study of Dispersive Tails

We have already mentioned that part of the evolution of a perturbed solitary-wave is the emergence of small amplitude, oscillatory wavetrains, the *dispersive tails*, that travel in both directions. In this subsection we study numerically the main features of dispersive tails for the Bona–Smith systems, and then, using the fact that they may be considered as approximate solutions of the associated linearized systems, we confirm some of their experimentally observed properties using the dispersion relations of the linearized equations.

We begin by presenting the experimental evidence for the dispersive tails produced by the evolution of the perturbed initial solitary-wave profile (2.1) for $r = 1.1$. By magnifying the graphs of Fig. 2 we obtain Figs. 5 and 6 that show in detail the dispersive tails for the η and u, respectively, components of the solution at $t = 100$. The solitary-wave travels to the right and the dispersive tail forms two wavetrains, one following the solitary-wave and travelling to the right, and another travelling to the left; by $t = 100$ the latter has wrapped itself around the boundary.

Table 1 Data of the leading pulse of the leftward-travelling η-dispersive tail and number of following positive pulses of height greater than 10^{-5}. (Evolution of Fig. 2)

t	x^*	Amplitude	Speed	Support	Pulses
10	−108.77189	0.03178			2
20	−118.44063	0.02832	0.967	28.2	4
30	−128.25563	0.02616	0.982	31.3	7
40	−138.13523	0.02463	0.988	33.9	9
50	−148.05173	0.02347	0.992	36.3	11
60	142.00776	0.02255	0.994	38.1	14
70	132.05035	0.02179	0.996	39.8	17
80	122.08037	0.02114	0.997	41.4	19
90	112.10066	0.02059	0.998	42.9	21
100	102.11320	0.02010	0.999	44.3	24

Table 2 Data of the leading pulse of the rightward-travelling η-dispersive tail and number of following positive pulses of height greater than 10^{-5}. (Evolution of Fig. 2)

t	x^*	Amplitude	Speed	Pulses
10				
20				3
30				6
40	−63.31347	0.00687		9
50	−53.50979	0.00649	0.980	11
60	−43.67607	0.00619	0.983	13
70	−33.82085	0.00594	0.986	15
80	−23.94943	0.00573	0.987	17
90	−14.06528	0.00554	0.988	19
100	−4.17086	0.00539	0.989	21

In Tables 1 and 2 we present various numerical data on the two wavetrains. Table 1 concerns the leading pulse of the leftward-travelling η-train. The first column lists the time instances of the measurements. The second contains the coordinate x^*, where the leading pulse gains its maximum, calculated using Newton's method with 10 iterations starting with the quadrature node (cf. Appendix 1) where the pulse has its maximum value ("discrete maximum"). The third column contains the values of the maximum height of the leading pulse, while the fourth column shows the speed of the leading pulse, defined as the average speed of x^*, and computed as $\Delta x^*/\Delta t$, where $\Delta t = 10$. The fifth column shows the "support" of the first pulse, defined as the wavelength of the full leading pulse, i.e. of its positive and negative part. Finally, the last column shows the number of observed positive pulses (that achieved maximum height greater than 10^{-5}) following the main pulse of the leftward-travelling train.

Table 2 shows some analogous data for the rightward-travelling η-dispersive tail. We have not measured the support of the leading pulse of the rightward-travelling

dispersive tail because its parameters are harder to measure due to its smaller size and somewhat slower development. Otherwise, the data of these tables confirm the basic characteristics of dispersive tails observed in one-way models such as the KdV equation, for example the eventual temporal decay of the maximum amplitude and of the amplitude of subsequent pulses, increase of the support of the pulses and of the number of pulses as t grows, etc. It is worthwhile to note that the speeds of the two leading pulses that travel to the left and to the right seem to have almost stabilized by $t = 100$. A least squares fit of the data describing the temporal decay of the maximum amplitude of the leftward-travelling leading pulse of the η-dispersive tail reveals that at least up to $t = 100$ the decay of the pulse is very accurately predicted by a decay law of the form $Ct^{-1/5}$.

In order to gain some theoretical understanding of the dispersive tails, we make the change of variable $y = x - c_s t$, where $c_s > 1$ is the speed of the solitary wave, and drop the nonlinear terms in the Bona–Smith system. The result is that small amplitude solutions of the system (like the dispersive tails) evolve, in a frame moving with the solitary wave, according to the linearized constant coefficient system

$$\begin{aligned} &(1 - b\partial_{yy})(\partial_t - c_s\partial_y)\eta + \partial_y u = 0, \\ &(1 - b\partial_{yy})(\partial_t - c_s\partial_y)u + \partial_y(1 + c\partial_{yy})\eta = 0. \end{aligned} \tag{2.2}$$

Combining equations in (2.2), we see that η (and u as well) satisfies the equation

$$(1 - b\partial_{yy})^2(\partial_t - c_s\partial_y)^2\eta - \partial_{yy}(1 + c\partial_{yy})\eta = 0, \tag{2.3}$$

which has solutions of the form $\eta(y, t) = \mathrm{e}^{\mathrm{i}(ky-\omega(k)t)}$, $k \in \mathbb{R}$, provided the dispersion relation

$$\omega_\pm(k) = -c_s k \pm \frac{k\sqrt{1 - ck^2}}{1 + bk^2}, \tag{2.4}$$

holds for the frequency $\omega(k)$. The (local) phase speed, relative to the speed of the solitary waves, is therefore given by the expression

$$v_\pm(k) = \frac{\omega_\pm(k)}{k} = -c_s \pm \frac{\sqrt{1 - ck^2}}{1 + bk^2}. \tag{2.5}$$

Recall that for the Bona–Smith systems $c = \frac{2}{3} - \theta^2$, $b = \frac{3\theta^2-1}{6}$ with $\theta^2 \in [2/3, 1]$. Hence, $-\frac{1}{3} \le c \le 0$, $\frac{1}{6} \le b \le \frac{1}{3}$, and $2b + c = \frac{1}{3}$. Therefore the function $\phi : [0, \infty) \to \mathbb{R}$, defined by $\phi(x) = \frac{\sqrt{1-cx}}{1+bx}$, $x \ge 0$, satisfies $\phi(0) = 1$ and is strictly decreasing to 0 as $x \to \infty$. We conclude from (2.5) that for all wavenumbers $k > 0$,

$$-(c_s + 1) < v_-(k) < -c_s < v_+(k) < -c_s + 1 < 0, \tag{2.6}$$

so that individual plane wave components of the dispersive tail of the form $\mathrm{e}^{\mathrm{i}(ky-\omega_+(k)t)}$ (i.e. that travel to the right) trail the solitary wave, and their absolute phase speed $v_+(k) + c_s$ is less than 1. Moreover, components corresponding to longer wavelengths (smaller wavenumbers k) are faster than those of shorter wavelength.

Components of the form $e^{i(ky-\omega_-(k)t)}$ (i.e. those travelling to the left, with absolute phase speed $|v_-(k)+c_s|$) have the same properties.

The associated group velocities $\omega'_\pm = \frac{d\omega_\pm}{dk}$ are given by the formulas

$$\omega'_\pm(k) = -c_s \pm \frac{1-(b+2c)k^2}{(1+bk^2)^2\sqrt{1-ck^2}}. \tag{2.7}$$

In the case of one-way model equations, such as KdV and BBM, the analogous group velocities turn out to be always negative, [26, 28], so that the dispersive tails are seen to be travelling to the left relatively to the solitary wave. In the case of a two-way model, such as a Boussinesq system, one can make further observations. For the Bona–Smith system at hand, since $b+2c = \frac{1}{6}(7-9\theta^2)$ in (2.7), we distinguish two cases:

(i) $\frac{7}{9} \le \theta^2 \le 1$: In this case, $b+2c \le 0$. Since $-(b+2c) \le b$, the function $\psi : [0,\infty) \to \mathbb{R}$ defined by $\psi(x) = \frac{1-(b+2c)x}{(1+bx)^2\sqrt{1-cx}}$ is positive and satisfies $\psi(x) \le 1$ for $x \ge 0$, because, for such x, $1-(b+2c)x \le (1+bx) \le (1+bx)^2\sqrt{1-cx}$. In addition, $\psi(x) \to 0$, $x \to \infty$. We conclude that for all wavenumbers $k > 0$,

$$-c_s - 1 < \omega'_-(k) < -c_s < \omega'_+(k) < -c_s + 1 < 0. \tag{2.8}$$

Hence, in the usual frame of reference (x,t) there are two dispersive groups, one travelling to the left and one to the right following the solitary-wave but with a group velocity smaller than c_s. This confirms e.g. the numerical results shown in Figs. 5, 6 and 7a, wherein $\theta^2 = \frac{9}{11}$.

(ii) $\frac{2}{3} \le \theta^2 < \frac{7}{9}$: In this case, $b+2c > 0$. The function ψ becomes negative for $x > 1/(b+2c)$, and satisfies $0 < \psi(x) \le 1$ for $0 \le x < 1/(b+2c)$, $\lim_{x\to\infty}\psi(x) = 0$. In addition, since $b+2c < b$, if $-\mu := \min_{x\ge 0}\psi(x)$, then $0 < \mu < 1$. We conclude that for the group velocities of the two wavetrains there holds, for all wavenumbers $k > 0$,

$$\begin{aligned} &-c_s - \mu \le \omega'_+(k) < -c_s + 1 < 0, \\ &-(c_s+1) < \omega'_-(k) \le -c_s + \mu < 0. \end{aligned} \tag{2.9}$$

Hence, e.g. in the usual frame of reference (x,t), we still have two dispersive groups, one travelling to the left and one to the right following the solitary-wave but with a group velocity smaller than c_s. In addition, for large k (specifically for $k^2 > (b+2c)^{-1} = 6/(7-9\theta^2)$, for which $\psi(k^2) < 0$), i.e. for small wavelengths, we have $\omega'_+ = -c_s + \psi(k^2) < -c_s - \psi(k^2) = \omega'_-$, i.e. a situation where the two groups do not tend to separate themselves.

As evidence of this phenomenon, contrast the region of "separation" between the two dispersive tails (near $x = -100$) in Figs. 7a and 7b.

Figure 7a is identical to a part of Fig. 5 (modulo changes in scale in both axes). Figure 7b is the graph of $\eta(x,t)$ at $t = 100$, computed numerically as the solution of the Bona–Smith system corresponding to $\theta^2 = 2/3$, i.e. of the BBM–BBM system. The initial profile for this evolution was a solitary-wave of the BBM–BBM system

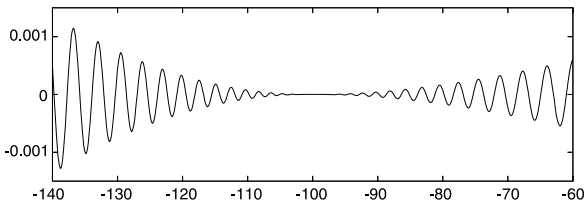

Fig. 7a Separation of dispersive tails, $\theta^2 = 9/11$

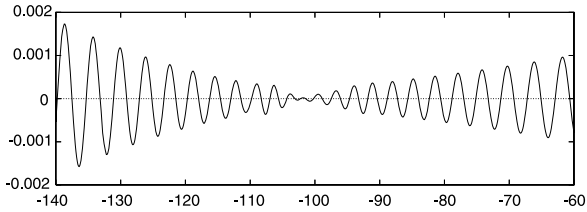

Fig. 7b Separation of dispersive tails, $\theta^2 = 2/3$

"cleaned" by the procedure outlined in Appendix 1 (recall that there are no analytical formulas for solitary waves for this system), whose η-component was perturbed again by a multiplicative factor of 1.1. In contrast to the practically "separated" dispersive tails of Fig. 7a, Fig. 7b indicates that there exists a region with small wavelength oscillations where the two tails seem to be interacting.

3 Effects of Larger Perturbations

When we increased the size of the perturbations of the exact solitary-wave profiles that we took as initial conditions in our numerical simulations, we observed, in many cases, that more solitary waves emerged as time grew. These solitary waves (followed by dispersive tails) travelled in general in both directions and interacted with each other, retaining their shape and speed. Occasionally, the initial perturbation was so large that it caused $1 + \eta(x, t)$ to become negative at some x and $t > 0$. In some of these cases, the solution apparently developed a singularity soon thereafter. In this section we describe some of these effects of larger "perturbations". (Summaries of the outcome of the numerical experiments that we performed appear in the tables of Appendix 2, wherein the above-mentioned apparent singularity is referred to as "blow-up".)

3.1 Resolution into Solitary Waves

Our computations suggest that for the two-way models under study we have *resolution* of appropriate arbitrary initial data into *sequences of solitary waves* (plus dispersive tails). In this, the Boussinesq systems under consideration resemble the theoretically well-understood case of the (integrable) KdV equation and the numerically well-studied non-integrable one-way models such as the BBM equation. Resolution into solitary waves is, of course, an attendant long-time phenomenon and may be related to the *stability* of the solitary-wave solutions of these systems.

Table 3 Number of emerging solitary waves ($t = 100$), with initial conditions (5.1)

r	3	4	5	6	7	8	9	10	11	12	14	16	25	36	49
$\rightarrow$	1+	2	2	2	2	2	2+	3	3	3	3	3+	4	5	5+
$\leftarrow$	1	1+	1+	2	2	2	2+	2+	3	3	3	3	4	5	5+

Table 4 Number of emerging solitary waves ($t = 100$), with initial conditions (5.3)

r	0.8	0.5	0.4	0.3	0.2	0.15
$\rightarrow$	1	2	2+	3+	3+	5+
$\leftarrow$	1	1+	1+	2+	2+	3+

For example, a typical case of perturbation of solitary waves that gives resolution into many solitary waves plus dispersive tails is Case I in Appendix 2, wherein the initial conditions are given by (2.1) with increasing r. For example, when $r = 7$, the resulting evolution is shown in the sequence of plots of Fig. 8. By $t = 20$ two pairs of solitary waves have formed and are travelling in opposite directions followed by dispersive tails. The left-travelling wavetrain reappears on the right due to periodicity, and the two leading solitary waves collide and interact for the first time at about $t = 68$. There follow other collisions and interactions between pairs of solitary waves travelling in opposite directions as well as interactions involving the dispersive tails.

The increase of the number of solitary waves is more pronounced when we perturb with factors $r < 1$ the "spread" parameter λ occurring in the argument of the sech^2 initial profile of $\eta_0(x)$ in Case III of Appendix 2 (cf. Table 12). Note that taking $r < 1$ increases, while $r > 1$ decreases the spread, and, consequently, the number of solitary waves into which the initial waveform is resolved. Figure 9 shows the evolution of an example of Case III, specifically that issuing from a perturbation of the spread of $\eta_0(x)$ with $r = 0.2$. We observe that by $t = 90$ at least three rightward-travelling and two leftward-travelling solitary waves have apparently been created; the latter have wrapped around the endpoints due to periodicity.

Tables 3 and 4 quantify these observations. In both tables we list the number of η-solitary waves travelling to the right ($\rightarrow$) and to the left ($\leftarrow$) that have clearly emerged by $t = 100$ for initial conditions of the form (5.1) and (5.3), respectively. (The symbol + in the tables indicates that an additional solitary-wave is probably being generated at $t = 100$.)

3.2 Interaction of Solitary Waves

Interactions between solitary waves have been thoroughly studied analytically and numerically in the case of integrable and nonintegrable one-way model equations. As is well-known the solitary waves emerge basically unchanged from the interaction; this property could be partly viewed as another manifestation of their stability. Similar studies of interactions may be performed numerically for two-way models, such as the Bona–Smith systems. For example, we consider again the evolution depicted in Fig. 8. Figure 10a shows the paths of the four emerging solitary waves up to $t = 150$

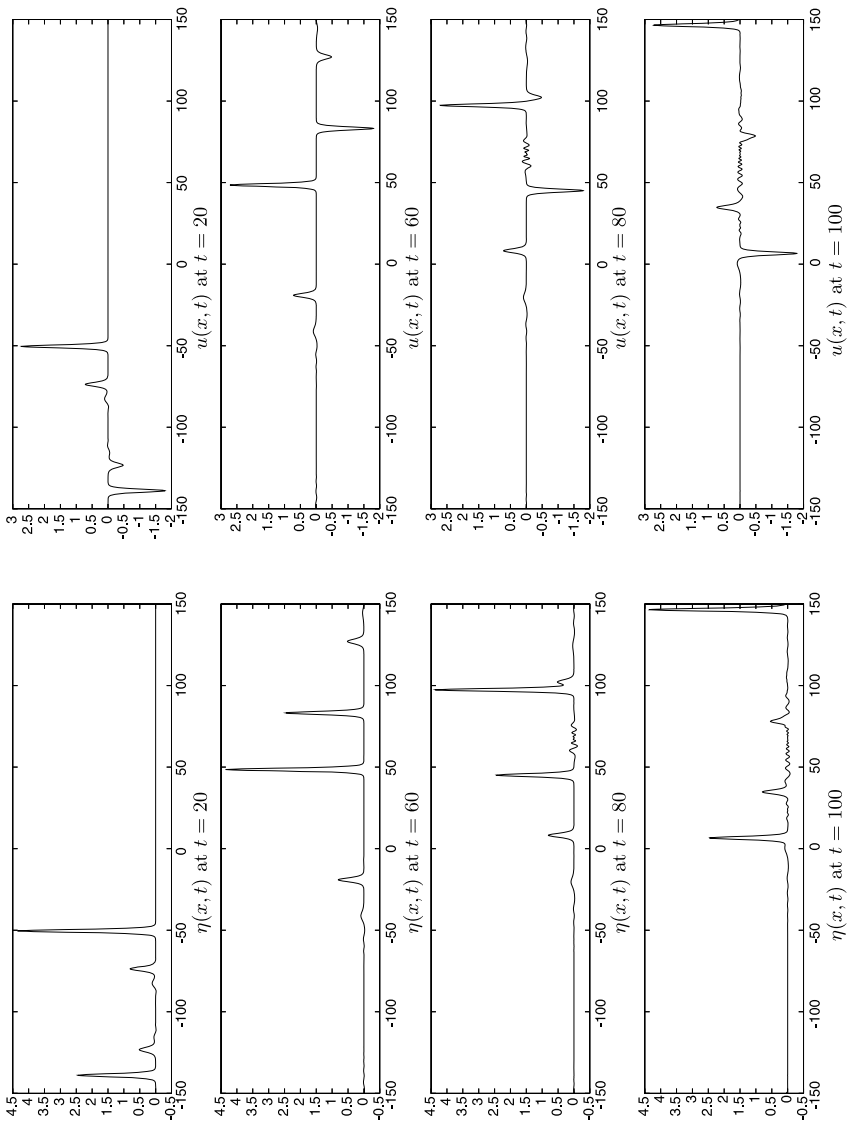

Fig. 8 Evolution of perturbed solitary wave, $\theta^2 = 9/11$. Initial conditions (5.1), $r = 7$

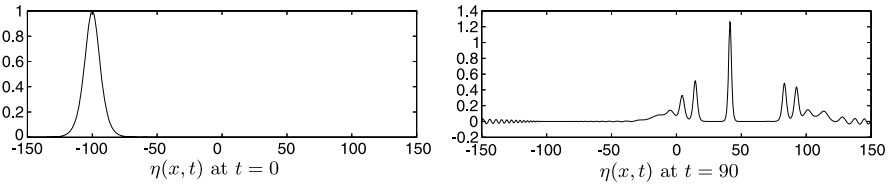

Fig. 9 Evolution of a perturbed solitary wave, Case III in Appendix 1. Perturbation of the spread parameter of $\eta_0(x)$, $r=0.2$

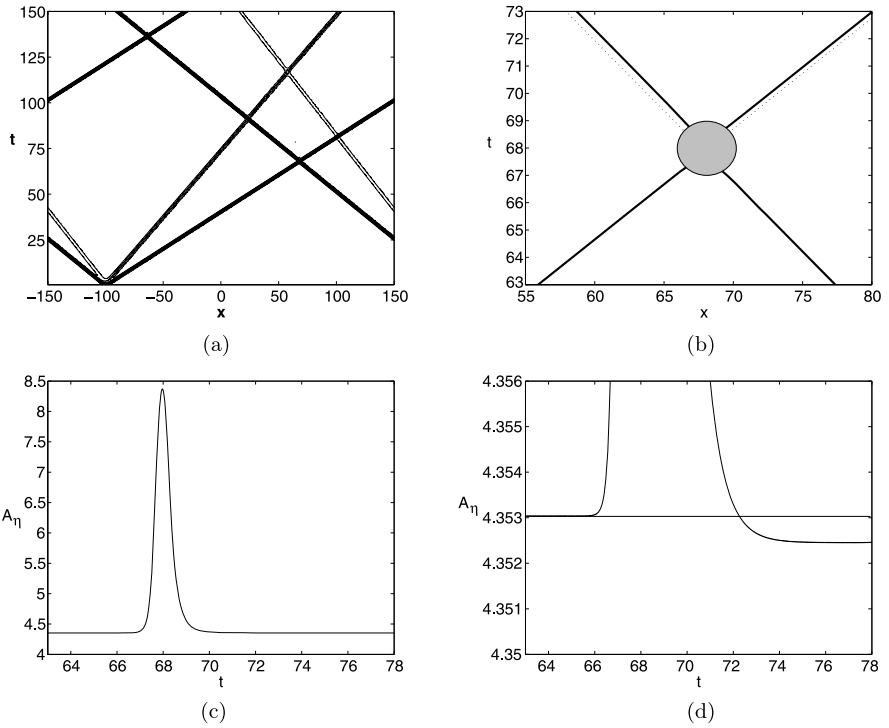

Fig. 10 Interaction of solitary waves. (Evolution of Fig. 8)

in an x, t diagram, while Fig. 10b–d depict some details of the head-on collision of the two larger solitary waves at about $t=68$. In Fig. 10b we plot the positions of the centers of these pulses (i.e. the points where they assume their maximum value) as functions of t before and after their collision. The solid lines are the actual positions, while the dotted lines would represent the paths if there were no interaction. (In this experiment the large solitary-wave is moving to the right with speed 2.473, while the small one is moving to the left with speed 1.947.) We observe that after their interaction both pulses are slightly delayed, suffering phase shifts opposed to their respective directions of motion. (For example, at $t=71$ the large solitary-wave has a phase shift equal to about 0.5882, while the phase shift of the small one is about 0.7921 spatial units.) Figure 10c shows the (total) amplitude A_η of the η component

of the solution as a function of t near the time of this interaction. The amplitudes $\eta_{\max}$ of the two solitary waves were equal to about 4.3530 and 2.7209 before the interaction and about 4.3525 and 2.7207 after the interaction. So, there is a small dip of the A_η value just after the interaction, shown more clearly in Fig. 10d which is a magnification of Fig. 10c. The maximum value of A_η was found to be about 8.3703, i.e. about 18% larger of the sum of the amplitudes of the waves before the interaction. The phase shifts and changes in amplitudes are nonlinear effects of the interactions of solitary waves and have been thoroughly studied for one way models. They have also been documented in the case of the BBM–BBM system in Bona and Chen [7] and in more detail for the Bona–Smith systems in [4].

3.3 Complex Interactions

The solitary waves also prove to be quite resilient when undergoing complicated interactions with large amplitude oscillations. A rather spectacular case is the interaction of Case V in Appendix 2, wherein the η-component of an exact solitary-wave is perturbed additively by a numerical noise function $p(x; m)$, cf. (5.5). For $m = 10^7$ the perturbation is quite substantial and the evolution of the η and u profiles is shown in Fig. 11. A single solitary-wave of amplitude $\eta_{\max} = 1.05820$ and $u_{\max} = 0.90937$ and speed $c_s = 1.4662$ emerges, followed by dispersive tails, as usual. We observe that a large-amplitude, high-frequency oscillatory wave packet forms in the region of interaction of the left- and right-travelling dispersive tails. The maximum amplitude of this packet (the u-component of which is of comparable height with that of the solitary wave) seems to be slowly diminishing in time. We let this experiment run up to $t = 300$ in order to observe the interaction of the (right-travelling) u solitary-wave with this irregular pulse. It is quite remarkable that the solitary-wave emerges unblemished from this interaction, with the exception of a phase shift (delay), which, in the temporal interval [240, 250], is equal to about 0.25 spatial units.

3.4 Blow-up of the Solution in Finite Time

As was already mentioned, in some cases, where appropriate perturbations of the initial solitary-wave were large enough, we observed that the solution developed a singularity in finite time. These types of perturbations correspond to "nonphysical" initial profiles, in a sense to be explained in the sequel, but it is important to note that there exist initial conditions for which the solution of Boussinesq systems under study apparently blow-up in finite time.

As an example, let us consider perturbations of the initial amplitude of u by a factor $r > 1$, cf. (5.2). The results of some experiments in this case are summarized in Table 11. For small values of r the initial waveform evolves into one solitary-wave travelling to the right, followed by a relatively small dispersive tail. There is also a dispersive "tail" that travels to the left which has a larger amplitude, the maximum value of which (for the η component of the solution) occurs at a negative excursion at the front of the oscillatory wavetrain. As r grows, this excursion becomes more negative, developing into a thin spike. For example, in the example shown in the sequence of graphs of Fig. 12, wherein $r = 3.3$, the excursion appears to approach but

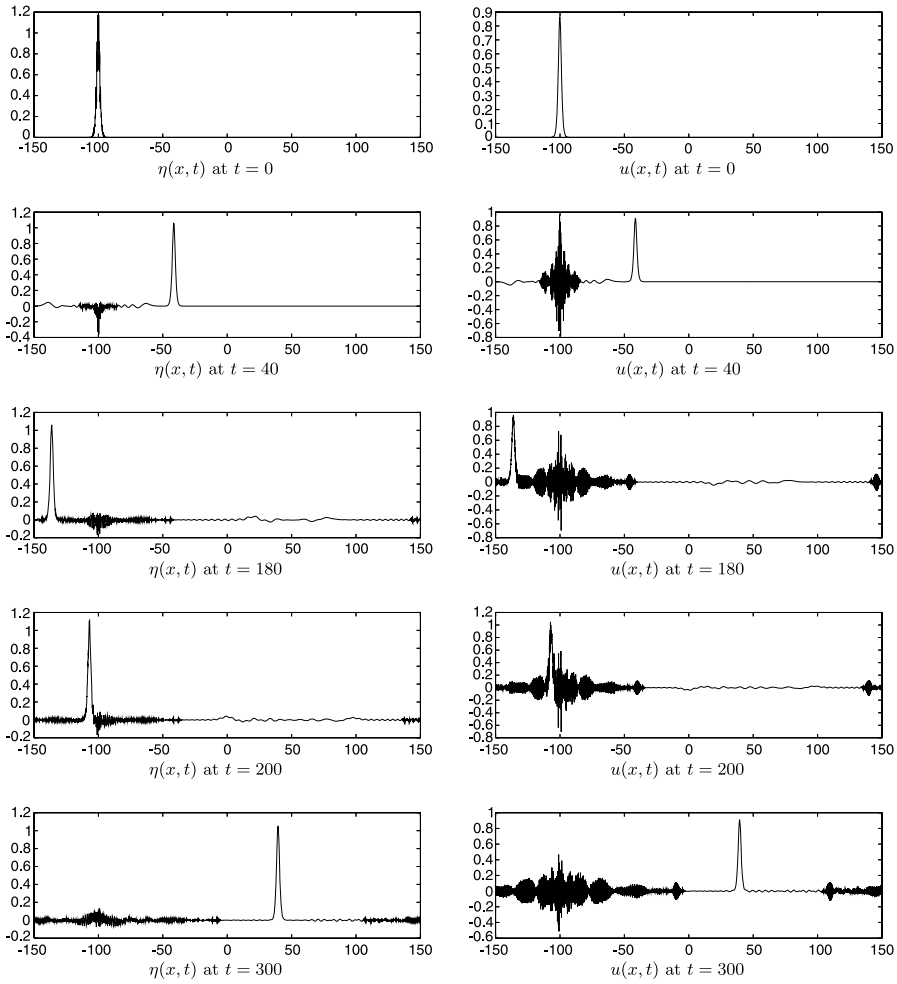

Fig. 11 Evolution of a perturbed solitary wave. Case V. Numerical noise in the initial condition of η, $m = 10^7$

not exceed -1 for $2 \le t \le 5$. Subsequently, the spike resolves itself into dispersive oscillations that spread as the front travels to the left and slowly diminish in amplitude.

As r increases further, it appears that the negative η-excursion becomes less than and stays below -1, and, subsequently, the solution blows up. (In particular, cf. Table 11, we observed no apparent blow-up up to $r = 3.6$ and blow-up for $r = 3.7$ and beyond.) For example, in the case $r = 3.8$ depicted in the sequence of Fig. 13, the negative η-peak that forms near $x = -100$ at $t = 3$ does not resolve into smaller amplitude oscillations; the solution apparently develops large-amplitude thin spikes that cause blow-up. The blow-up appears to be genuine and not an artifact of the numerical simulation: When repeated with smaller h and k, the computation yielded similar results. Of course, a more categorical answer and a detailed numerical description of

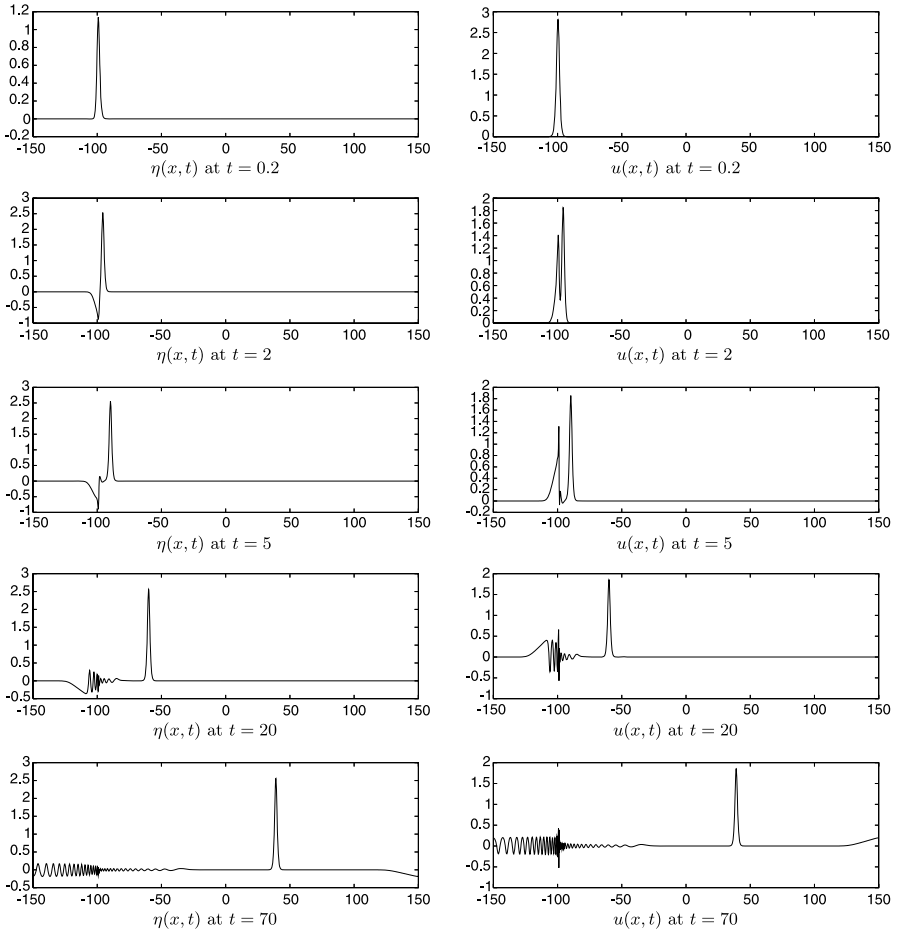

Fig. 12 Evolution of a perturbed solitary wave. Case II, $r = 3.3$

the blow-up requires a code that adaptively refines the time step and the spatial mesh-length around the singularity. We intend to study this question in the future using the adaptive mesh refinement strategy proposed in [10].

Recall that, in terms of the variables used in the system (1.1), the level $y = -1$ represents the bottom of the channel. Thus, a situation where $1 + \eta(x, t) < 0$ for some (x, t) is nonphysical and corresponds to local drying of the channel. It appears that increasing the size of the initial velocity profile of the solitary-wave by a large-enough multiplicative factor imparts to the water column a large push, which may empty the channel behind the wave. (A qualitatively similar phenomenon of blow-up occurs for perturbations wherein the initial η and u solitary profiles are multiplied by factors r_1 and r_2, respectively: We observed that blow-up occurs—again as a result of a strong negative excursion of the left-travelling η-dispersive wavetrain—when r_2 is sufficiently large compared with r_1.)

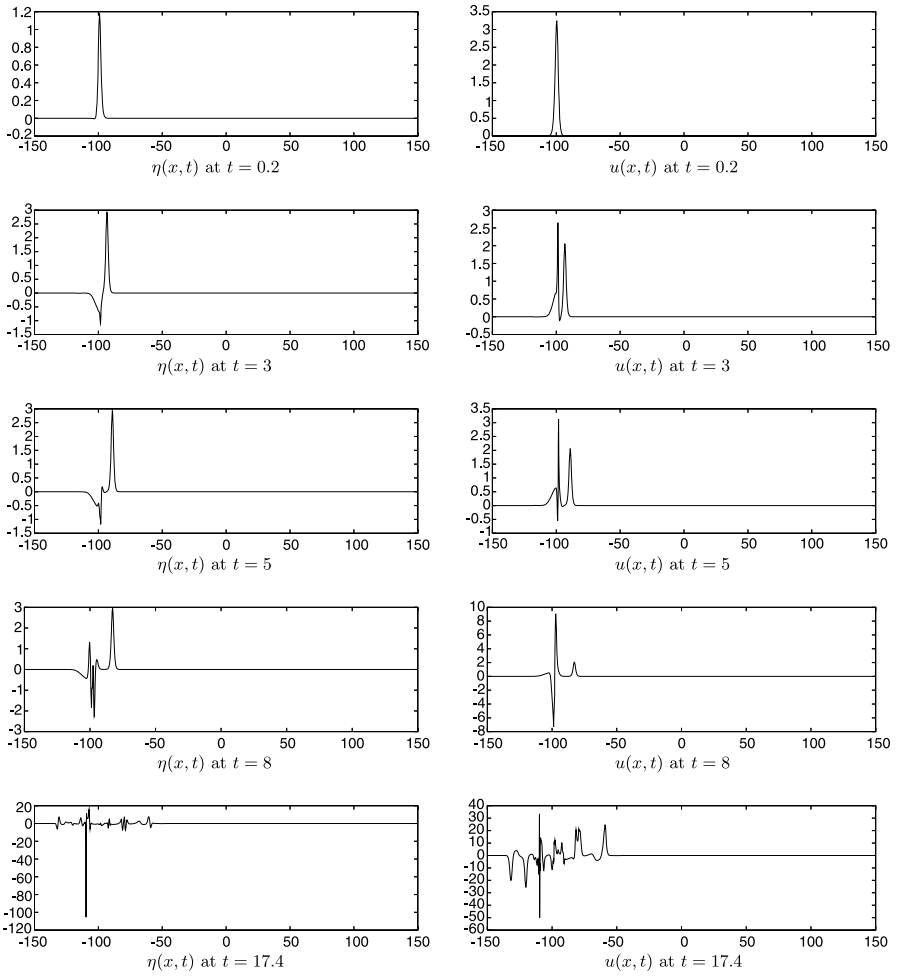

Fig. 13 Evolution of a perturbed solitary-wave toward apparent blow-up. Case II, $r = 3.8$

It is evident by the form of the invariant E, cf. (1.9), of this class of systems that the condition that $1 + \eta(x,t) < 0$ for some (x,t) is necessary for blow-up. Indeed, for solutions that are initially smooth and for which $1 + \eta(x,t) > 0$ for all x and $0 \leq t \leq T$, the positivity of the invariant guarantees that η is bounded in H^1, and hence in L^∞, up to $t = T$. It appears, though, that $1 + \eta$ becoming negative at some point x at some time $t > 0$ is not by itself sufficient to ensure subsequent blow-up of the solution. A case in point is furnished by the evolution corresponding to appropriate nonsymmetric perturbations of the initial data, as e.g. in Case VI in Appendix 2. Here η is perturbed initially by a smooth step-type factor as in (5.6a) and forms a pulse with a negative and a positive excursion if $\mu > 1$. If μ is not large enough, the initial η profile is resolved into two wavetrains, one travelling to the right consisting of a solitary-wave (the parameters of which are shown in Table 15) plus a dispersive tail, and one travelling to the left consisting of just a larger dispersive tail for μ up to

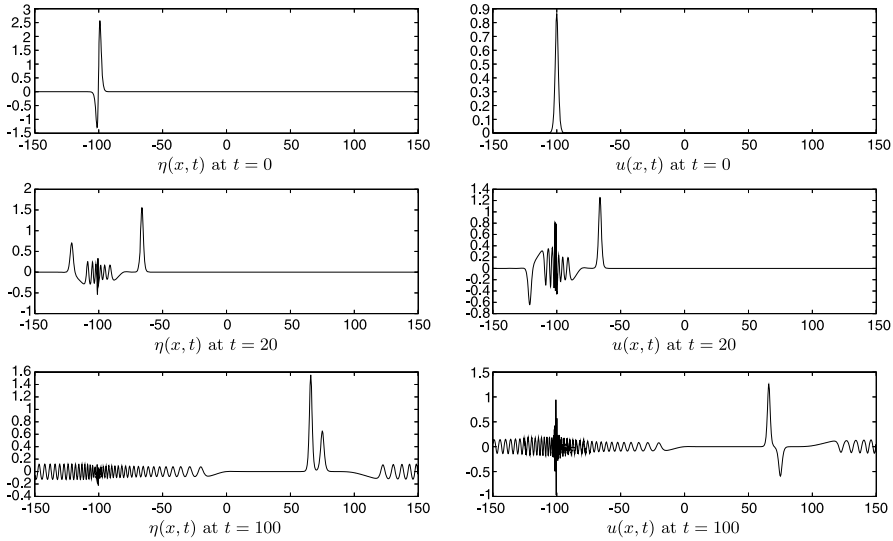

Fig. 14 Evolution of a perturbed solitary wave. Case VI(a), $\mu = 6$

about 2 and, for larger values of μ, of a small solitary-wave followed by a relatively large dispersive tail.

For $\mu = 6$, $\eta(x, 0)$ is less than -1 for x less than and close to -100. Nevertheless, this initial condition does not apparently lead to blow-up. As the sequence of graphs of Fig. 14 shows, there is considerable interaction of the large-amplitude dispersive tails, which seems to be diminishing as time increases. The interaction of the corresponding dispersive tails in the evolution of u is more violent but not catastrophic. For μ up to 6.25, we did not observe blow-up either. However, for $\mu = 6.28$, the solution apparently blows up. Figure 15 shows the evolution when $\mu = 6.3$.

In addition to those already mentioned, other types of large perturbations of sech^2-like initial data also lead to apparent blow-up of the solution of the system in finite time. These are not listed in Appendix 2, but include random noise perturbations of $\eta_0(x)$ of large size, sinusoidal perturbations of $\eta_0(x)$ of large enough amplitude and frequency, and suitable nonsymmetric perturbations of $u_0(x)$, respectively of $\eta_0(x)$, coupled with perturbations of the amplitude of $\eta_0(x)$, respectively of $u_0(x)$. In all these cases (including of course those of Tables 11 and 15, 16) we made the following observations regarding the blow-up:

1. As was already mentioned, the condition $\eta(x, t) < -1$ for some x and t is not sufficient for blow-up.
2. Initial data for which the inequality (1.8) is not satisfied do not necessarily lead to blow-up. In fact, the energy (1.9) may become quite large without any evidence of loss of existence of smooth solutions.
3. The transition to blow-up, as the perturbation parameters are varied, seems to be quite abrupt.
4. The invariant E, (1.9), can be written as $E = I_1 + I_2$, where $I_1(t) = \int_{-L}^{L} (\eta^2 + (\theta^2 - \frac{2}{3})\eta_x^2)\,\mathrm{d}x$ is equivalent, for $\theta^2 > 2/3$, to the square of the H^1 norm of η,

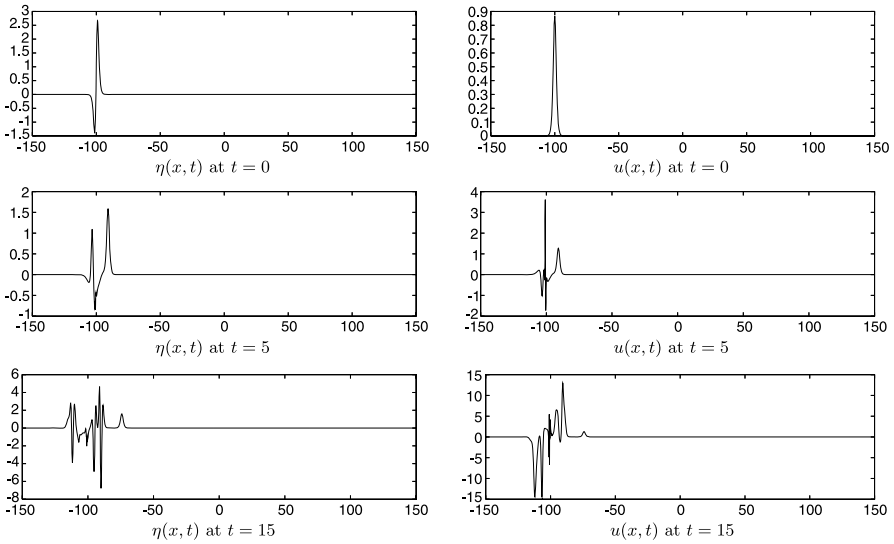

Fig. 15 Evolution of a perturbed solitary wave toward apparent blow-up. Case VI(a), $\mu = 6.3$

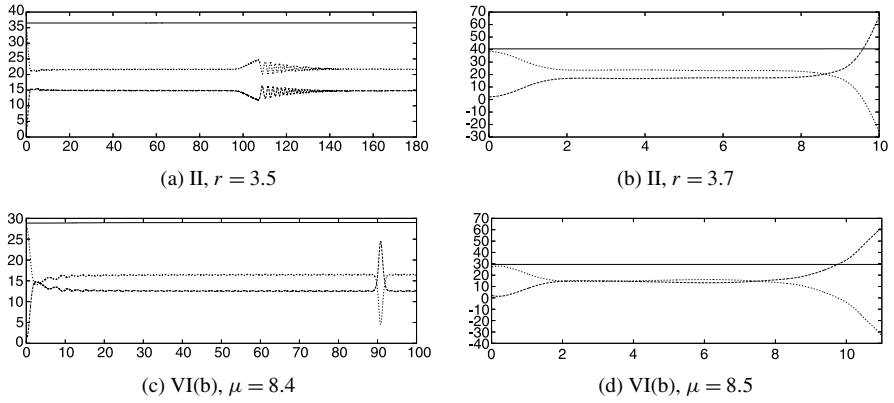

Fig. 16 E, I_1, I_2 as function of t in four cases. $E(t)$: ——, $I_1(t)$: - - - -, $I_2(t)$: ·····

and $I_2(t) = \int_{-L}^{L}(1+\eta)u^2\,\mathrm{d}x$. In all cases of apparent blow-up we observed that, after some temporal instance $t_* > 0$ prior to blow-up, the quantity $I_2(t)$ becomes monotonically decreasing, eventually assuming negative values. (As a result, of course, the H^1 norm increases.) This is illustrated in Fig. 16. Figure 16a shows E, I_1, I_2 as functions of t in Case II, $r = 3.5$ (no blow-up), while the analogous graphs of Fig. 16b (blow-up) correspond to initial conditions of the type (5.2) with $r = 3.7$, cf. Table 11. The oscillations observed in Fig. 16a for t approximately between 100 and 140 are due to the interaction of the main pulse with the dispersive tail. Figure 16c corresponds to initial perturbations of the type (5.6b) for $\mu = 8.4$ for which a smooth solution exists, at least up to $t = 100$. The curious temporary "exchange" of magnitudes of I_1 and I_2 just after $t = 90$ is due to an

interaction of pulses near that time value. The behavior of I_1, I_2 in the blow-up case corresponding to $\mu = 8.5$ is shown in Fig. 16d.

Appendix 1: Numerical Method

The numerical experiments on the stability of solitary waves of the Bona–Smith system that were presented in Sects. 2 and 3 were performed by a Galerkin-finite element full discretization of the initial-periodic boundary-value problem for the system. The scheme employed cubic splines for the spatial discretization coupled with time-stepping with the classical, explicit, fourth-order Runge–Kutta method. In this appendix we state the scheme and relevant available convergence results and make a computational assessment of its accuracy, paying particular attention to approximating and isolating solitary waves and measuring their parameters.

The numerical method is a standard Galerkin scheme on the space S_h of smooth, periodic, cubic splines with respect to a uniform mesh on $[-L, L]$ with meshlength h. We approximate the solution (η, u) of the Bona–Smith system (1.4, 1.5) by $(\eta_h, u_h) : [0, T] \to S_h \times S_h$, satisfying for $0 \le t \le T$ the semidiscrete equations

$$\begin{aligned} &\mathcal{A}(\eta_{ht}, \chi) + (u_{hx}, \chi) + ((\eta_h u_h)_x, \chi) = 0, \quad \forall \chi \in S_h, \\ &\mathcal{A}(u_{ht}, \varphi) + (\eta_{hx}, \varphi) + (u_h u_{hx}, \varphi) - c(\eta_{hxx}, \varphi') = 0, \quad \forall \varphi \in S_h. \end{aligned} \tag{4.1}$$

Here, we denote by $(\varphi, \chi) = \int_{-L}^{L} \varphi(x)\chi(x)\,dx$ the L^2 inner product and by $\|\cdot\| = (\cdot,\cdot)^{1/2}$ the L^2 norm on $[-L, L]$, and put $\mathcal{A}(\varphi, \chi) := (\varphi, \chi) + b(\varphi', \chi')$. We take as initial values for the o.d.e. system (4.1) the functions

$$\eta_h(0) = \Pi_h \eta_0, \quad u_h(0) = \Pi_h u_0, \tag{4.2}$$

where $\Pi_h v$ denotes any of a number of reasonable approximations of v in S_h (e.g. interpolant, L^2- or elliptic projection, etc.), for which there holds that

$$\|v - \Pi_h v\| = O\big(h^4\big),$$

given any function v in the (periodic) Sobolev space $H^4_\pi[-L, L]$. Then, it can be shown, cf. [2, 4], that the initial-value problem (4.1, 4.2) has a unique solution on $[0, T]$, which satisfies

$$\max_{0\le t\le T} \big(\big\|\eta(t) - \eta_h(t)\big\| + \big\|u(t) - u_h(t)\big\|\big) \le Ch^4,$$

where by C we shall denote positive constants independent of the discretization parameters.

The system of o.d.e's (4.1, 4.2) is discretized in the temporal variable by the classical, explicit, fourth-order Runge–Kutta scheme. Let J be a positive integer and define the time step $k := T/J$ and the time levels $t^n := nk$, $n = 0, 1, 2, \ldots$. It turns out that the system (4.1, 4.2) is not stiff; indeed, it may be shown, [2, 4], that the resulting fully discrete scheme is stable in L^2, and that the fully discrete approximations

$(\eta_h^n, u_h^n) \in S_h \times S_h$ of $(\eta(t^n), u(t^n))$ satisfy the error estimate

$$\max_{0\le n\le J}\left(\left\|\eta_h^n - \eta\left(t^n\right)\right\| + \left\|u_h^n - u\left(t^n\right)\right\|\right) \le C\left(k^4 + h^4\right),$$

unconditionally, i.e. without the need of any relation between k and h. As starting values we take $\eta_h^0 = \Pi_h \eta_0$, $u_h^0 = \Pi_h u_0$.

We refer the reader to [2, 4] for computational verification of the spatial and temporal rates of convergence of this numerical scheme as well as for a detailed computational study of its accuracy in approximating solitary waves; the latter includes computing several error indicators that are pertinent (cf. [10]) to assessing the fidelity of numerical approximations of exact solitary-wave solutions, such as their normalized amplitude, speed, phase and shape errors, and the errors in the values of the numerically computed invariants (1.9) and (1.19).

In the course of the numerical experiments testing the stability of solitary waves in the main body of the paper, it was observed that initial data of the type of perturbed solitary waves resolves itself, as t grows, into localized pulses resembling solitary waves plus oscillatory dispersive tails. In order to be reasonably certain that these localized pulses are indeed solitary waves, one must isolate them and check that they travel with practically constant speed and amplitude, retaining their shape. This may be accomplished in two different ways: One can perform a sufficiently long time simulation on a sufficiently large spatial interval in order to isolate a solitary wave, after it distances itself from its dispersive tail and before it interacts with other features of the solution. This sometimes may require a very large spatial interval, and the computational cost needed to maintain accuracy may become prohibitively large. As an alternative, one may "clean" the approximate solitary waves by an iterative process, as done e.g. in [7]. We present here examples of both procedures in order to give the reader a sense of their accuracy.

If we perturb the η-component of the exact solitary-wave profile $(\eta_s(x,0), u_s(x,0))$ given by (1.15, 1.16) for $\theta^2 = 9/11$ and $x_0 = 100$ by a factor equal to 1.8, i.e. use as initial conditions the functions $\eta_0(x) = 1.8\eta_s(x,0)$ and $u_0(x) = u_s(x,0)$, and integrate forward in time using the finite element scheme with $h = 0.1$, $k = 0.01$, we observe that the initially perturbed solitary wave gives rise to two wavetrains travelling in opposite directions. The rightward-travelling wavetrain consists of a main pulse resembling a solitary wave, whose η-component has an amplitude of about 1.48 and a speed of about 1.62, and is followed by an oscillatory dispersive tail. The leading pulse has clearly separated from the tail by $t = 40$. The leftward-travelling wavetrain also develops a leading pulse, which, at $t = 80$, after having wrapped itself around the boundary, is travelling with an η-amplitude and speed approximately equal to 0.25 and 1.12, respectively, and is just beginning to detach itself from its dispersive tail. Figure 17 shows the solution profile at $t = 80$.

Isolating the large approximate solitary wave is not hard. For $t \in [40, 90]$ it has sufficiently outrun its dispersive tail and has not yet interacted with the small solitary wave. Table 5 shows the amplitudes A_η and A_u at the indicated values of $t = t^n$ of the numerical solution η_h^n, u_h^n in this temporal interval, as well as the values of the speed c_h of the large pulse at t^n. These parameters were computed as follows. Given n, in order to find e.g. the point x^* where η_h^n achieves its maximum $(A_\eta(t^n) := \eta_h^n(x^*))$, we

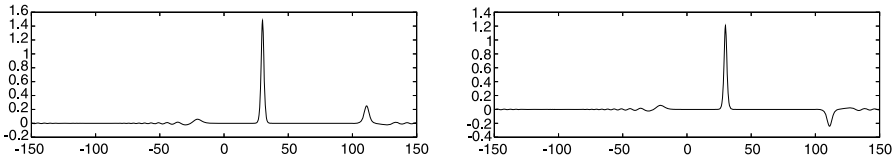

Fig. 17 Evolution of a perturbed solitary wave at $t = 80$. *Left*: $\eta(x,t)$. *Right*: $u(x,t)$

Table 5 Amplitudes A_η, A_u and speed c_h of the large solitary wave of Fig. 17 without cleaning

t^n	40	60	80	90
A_η	1.480435	1.480435	1.480435	1.480434
A_u	1.206309	1.206309	1.206309	1.206308
c_h	1.62419	1.62419	1.62420	1.62419

Table 6 Amplitudes A_η, A_u and speed c_h of the large solitary wave of Fig. 17 after cleaning

t^n	0	20	40	60	80	100
A_η	1.480434	1.480434	1.480435	1.480435	1.480434	1.480434
A_u	1.206308	1.206309	1.206309	1.206309	1.206308	1.206308
c_h	–	1.62419	1.62419	1.62420	1.62420	1.62419

define first an initial approximation x_0^* of x^* as that quadrature node at which η_h^n is maximized relatively to its values at the quadrature nodes. (We use Gauss quadrature with five nodes per mesh interval for computing the integrals in the finite element scheme.) Taking x_0^* as starting value, we compute x^* by Newton's method with a few iterations, as the nearby root of the equation $\frac{\mathrm{d}}{\mathrm{d}x}\eta_h^n(x) = 0$. The speed $c_h(t^n)$ is computed as the quotient $\frac{x^*(t^n)-x^*(t^n-10)}{10}$. (The temporal interval $\Delta t = 10$—an integer multiple of k in our computations—in this difference quotient proved sufficiently large for the purpose of smoothing away oscillations in the discrete approximations of the speed.)

In order to check these values, we also "clean" the large solitary wave. At $t = 90$ we cut the large wave off the rest of the solution by setting η_h, u_h equal to zero in the intervals $[-150, 27]$ and $[67, 150]$, centered it at $x = -100$ by translation, and took the resulting pair of functions as new initial conditions for the system. We integrated then up to $t = 100$, observing that during this run the amplitude of the oscillatory noise behind the wave was less than 5×10^{-10}, the noise threshold value used in this paper for pronouncing an approximate solitary wave "clean". The amplitudes A_η, A_u of η and u, and the speed c_h of the cleaned wave as functions of t are shown in Table 6. Note that the entries in Tables 5 and 6 agree quite well. We also computed a kind of normalized "shape" error for the approximate "cleaned" solitary wave relative to its initial value. This error was defined as $\inf_y \|\eta_h^n(\cdot) - \eta_h^0(\cdot - y)\|/\|\eta_h^0\|$, where $\eta_h^0 \in S_h$ was the cleaned solitary wave centered at $x = -100$ and taken as initial value (with the corresponding u_h^0) for the computation that yielded η_h^n at $t = t^n$. We

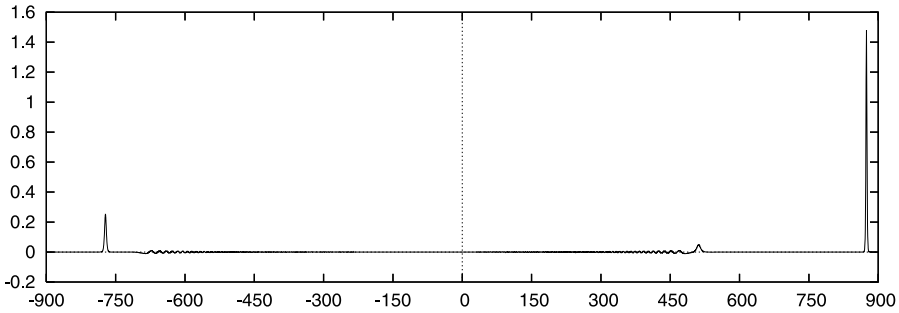

Fig. 18 $\eta(x,t)$ at $t=600$. $(L=900)$

Table 7 Amplitudes A_η, A_u and speed c_h of the small solitary wave without cleaning. $(L=900)$

t^n	500	520	540	560	580	600
A_η	0.25022509	0.25022509	0.25022510	0.25022511	0.25022509	0.25022509
A_u	0.24129404	0.24129403	0.24129404	0.24129405	0.24129404	0.24129403
c_h	1.121307	1.121308	1.121308	1.121307	1.121308	1.121308

computed it as $\zeta(y^*)$, where y^* was the root of the equation $\frac{\mathrm{d}}{\mathrm{d}y}\zeta^2(y)=0$, $\zeta(y):=\|\eta_h^n-\eta_h^0(\cdot-y)\|/\|\eta_h^0\|$, found by Newton's method with a few iterations and initial guess $y^0=c_h(t^{n-1})t^{n-1}$. The maximum value of this error for $10\le t^n\le 100$ was about 1.218×10^{-5}. It is interesting to note that substituting $A_\eta=1.48043$ and $A_u=1.20631$ for $\eta(0)$, $u(0)$, respectively, in the exact speed–amplitude relation (1.14) for solitary waves, we obtain a speed value of about 1.624193, which differs from the value of c_h in Table 5 by an amount of the order 10^{-6}.

The small solitary wave in Fig. 17 is much harder to isolate or clean, as the spatial interval $[-150,150]$ is not large enough, and, consequently, the small solitary wave is not able to separate itself from the large solitary wave and the rest of the rightward-travelling wave train. In order to isolate it, we solved the same problem (using the same initial conditions, numerical method, and mesh sizes) on the interval $[-900,900]$. By $t=600$ (cf. Fig. 18), the small solitary wave is seen to be approaching the boundary $x=-900$, having distanced itself considerably from its trailing dispersive tail. (It is interesting to observe that a *third* solitary wave, of height about 0.07, is apparently emerging at this larger t at the head of the rightward-travelling oscillatory wavetrain.) Without cleaning the solitary-wave travelling to the left, we record in Table 7 its parameters during the temporal interval $[500,600]$.

Alternatively, we "clean" the small solitary wave in the interval $[-500,500]$. At $t=280$ the small solitary wave (travelling to the left) has not yet reached the boundary $x=-500$. At this point we cut the small solitary wave and its dispersive tail from the rest of the solution by setting η_h and u_h equal to zero in the interval $[-100,437.5]$, cf. Fig. 19a. It should be noted that "cutting", i.e. setting $\eta_h,u_h=0$ in an interval, is done *smoothly* by setting the coefficients of the cubic B-spline basis function $\{\phi_j\}$ in the representation of η_h and u_h equal to zero after

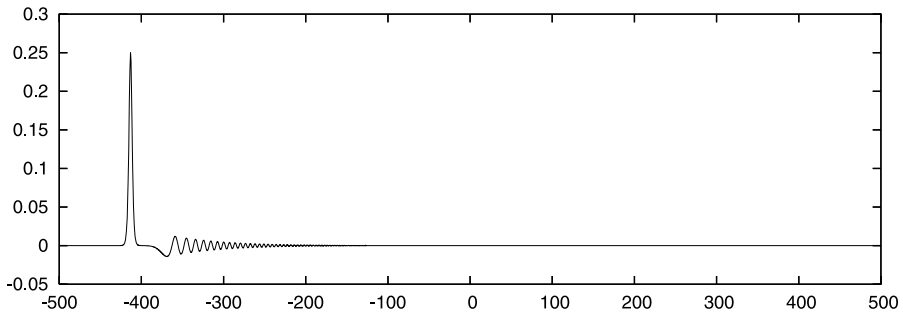

Fig. 19a Small η-wave after 1st cut ($L = 500$)

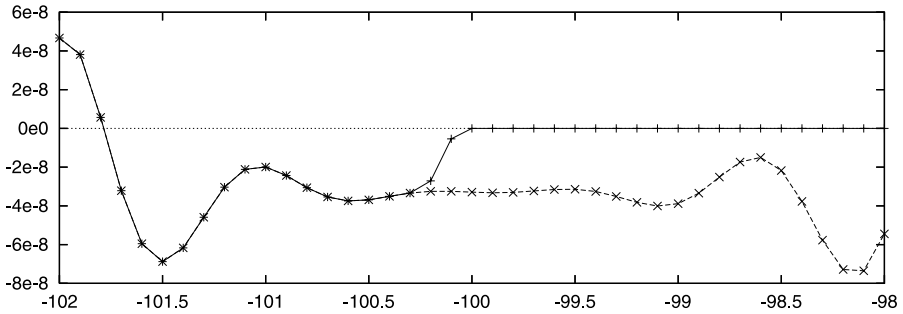

Fig. 19b Magnification of Fig. 19 in the interval $[-102, -98]$. (*Solid line*, $+$: after cut, *dashed line*, $\times$: before cut)

Table 8 Amplitudes A_η, A_u and speed c_h of the small solitary wave after the first cleaning. ($L = 500$)

t^n	0	40	80	100	200	260
A_η	0.25022524	0.25022514	0.25022509	0.25022509	0.25022511	0.25022510
A_u	0.24129418	0.24129408	0.24129404	0.24129404	0.24129405	0.24129404
c_h	—	1.121307	1.121307	1.121308	1.121307	1.121308

some suitable index. In the present case, for example, let $x_{i+1} = -100$. Then, if, say, $\eta_h = \sum_{j=1}^{N} c_j \phi_j(x)$ at $t = 280$, we put $c_j = 0$ for $j \geq i$. Hence, the B-spline of the largest index present in the representation of η_h after the cut is $\phi_{i-1}(x)$, centered at $x_{i-1} = -100.2$, which has the value zero (as do its first and second derivatives) at $x_i = -100$; see Fig. 19b. The same cutting is applied to u_h.

We now use the solution that remains after the first cleaning as the new initial value and let it evolve (it continues travelling to the left and wraps around the boundary) up to $t = 260$. During this evolution we measure the amplitude of η and u and the speed of the small solitary wave. These values are shown in Table 8.

We repeat this procedure two more times: We cut (truncate smoothly) η_h and u_h in appropriate intervals, let the small solitary-wave travel, then cut again, and so on. After the third cleaning, the amplitude of the residue behind the wave is about 10^{-12},

Table 9 Amplitudes A_η, A_u and speed c_h of the small solitary wave after the third cleaning. ($L = 500$)

t^n	0	40	100	200	300	400
A_η	0.25022511	0.25022509	0.25022509	0.25022509	0.25022511	0.25022510
A_u	0.24129405	0.24129403	0.24129404	0.24129403	0.24129405	0.24129404
c_h	–	1.121308	1.121308	1.121308	1.121307	1.121307

well below the cleaning threshold 5×10^{-10}. During the last evolution, in a temporal interval of 400 units, the amplitudes and speed had the values shown in Table 9.

Comparing Tables 8 and 9 reveals that we have not gained much by the extra cleanings, in the sense that we obtain identical amplitudes if we round them to six decimal digits, and identical speeds rounded to five decimal digits. (The only solid gain is the stabilization of the seventh digit (0) of A_u.) Comparing with Table 7 shows that both procedures give that the parameters of the small solitary wave of Fig. 17 are $A_\eta = 0.2502251$ (last digit by rounding), $A_u = 0.2412940$ (last digit exact), $c_h = 1.12131$ (last digit by rounding). Substituting these values of A_η and A_u in the relation (1.14), we obtain a speed value of 1.12130755. We also note that the typical maximum normalized "shape" error for the small solitary-wave produced by these runs was about 1.5×10^{-6}. These values represent in essence the limit resolution possible with our numerical method and mesh sizes $h = 0.1$, $k = 0.01$. More digits may be gained by using high-order methods and smaller mesh sizes.

It should finally be noted that all computations in this appendix and in Sects. 2 and 3 were checked by parallel runs performed with a pseudospectral code. In all cases the computed values of the parameters of the solitary waves (amplitude, speed, etc.) obtained by both schemes were identical, to the digits shown.

Appendix 2: Types of Perturbations

We have experimented with many types of perturbations of initial solitary-wave profiles. For each type we used perturbations of several magnitudes. In what follows, we summarize the outcome of some of the experiments that we performed. We show only cases to which reference has been made in the text of the paper; a description of the full set of experiments is included in a technical report available from the authors upon request. The tables show the numerically computed amplitudes $\widetilde{\eta}_{\max}$, $\widetilde{u}_{\max}$ and speed $\widetilde{c}_s$ of the largest emerging solitary wave, and the number of leftward-($\leftarrow$) and rightward-($\rightarrow$) travelling solitary waves that have formed by $T = 100$. The symbol $\alpha+$ indicates that, by $T = 100$, α solitary waves have definitely appeared and one more is probably being generated. (Isolating the latter would require following it over a much larger temporal and spatial interval, something that we did not do.)

Table 10 Case I

r	$\tilde{\eta}_{\max}$	$\tilde{u}_{\max}$	$\tilde{c}_s$	$\rightarrow$	$\leftarrow$
0.7	0.81470	0.72360	1.3688		
1.001	1.00061	0.86648	1.4436	1	
1.01	1.00612	0.87062	1.4458	1	
1.1	1.06110	0.91152	1.4673	1	
1.2	1.12188	0.95608	1.4909	1	
1.5	1.30240	1.08466	1.5591	1	
1.6	1.36201	1.12594	1.5811	1	0+
1.8	1.48043	1.20631	1.6242	1	1
2.3	1.77237	1.39589	1.7266	1	1
2.5	1.88768	1.46771	1.7657	1+	1
2.7	2.00225	1.53748	1.8038	1+	1
3.0	2.17282	1.63862	1.8594	1+	1
7.0	4.35303	2.72091	2.4729	2	2

I. Perturbation of the Amplitude of η

We integrate the Bona–Smith system with $\theta^2 = 9/11$, taking as initial conditions:

$$\begin{aligned} \eta_0(x) &= r\eta_0 \operatorname{sech}^2\big(\lambda(x+x_0)\big), \\ u_0(x) &= B\eta_0 \operatorname{sech}^2\big(\lambda(x+x_0)\big), \end{aligned} \tag{5.1}$$

where $\eta_0 = 1$, $B = \sqrt{3}/2$, $\lambda = \frac{1}{4}\sqrt{33/5}$, $x_0 = 100$. The unperturbed solitary-wave ($r = 1$) travels to the right with speed $c_s = 5\sqrt{3}/6 \cong 1.443376$. Table 10 shows the results for several values of the perturbation factor.

II. Perturbation of the Amplitude of u

Bona–Smith system, $\theta^2 = 9/11$. Initial conditions:

$$\begin{aligned} \eta_0(x) &= \eta_0 \operatorname{sech}^2\big(\lambda(x+x_0)\big), \\ u_0(x) &= rB\eta_0 \operatorname{sech}^2\big(\lambda(x+x_0)\big), \end{aligned} \tag{5.2}$$

η_0, B, λ, x_0 as in Case I.

III. Perturbation of the "Spread" Parameter λ of η

Bona–Smith system, $\theta^2 = 9/11$. Initial conditions:

$$\begin{aligned} \eta_0(x) &= \eta_0 \operatorname{sech}^2\big(r\lambda(x+x_0)\big), \\ u_0(x) &= B\eta_0 \operatorname{sech}^2\big(\lambda(x+x_0)\big), \end{aligned} \tag{5.3}$$

η_0, B, λ, x_0 as in Case I. Note that $r > 1$ decreases and $r < 1$ increases the spread of $\operatorname{sech}^2(r\lambda x)$.

Table 11 Case II

r	$\tilde{\eta}_{\max}$	$\tilde{u}_{\max}$	$\tilde{c}_s$	$\rightarrow$	$\leftarrow$
0.7	0.81904	0.72702	1.3706	1	
1.1	1.06157	0.91186	1.4675	1	
2.1	1.70980	1.35622	1.7051	1	
3.3	2.56101	1.85773	1.9809	1	
3.5	2.71020	1.93825	2.0258	1	
3.6	2.78555	1.97819	2.0484	1	
3.7	blow-up	blow-up			

Table 12 Case III

r	$\tilde{\eta}_{\max}$	$\tilde{u}_{\max}$	$\tilde{c}_s$	$\rightarrow$	$\leftarrow$
0.2	1.26042	1.05525	1.5434	3+	2+
0.5	1.15330	0.97886	1.5029	2	1+
0.8	1.05576	0.90757	1.4652	1	1
1.1	0.97475	0.84702	1.4334	1	
2	0.80849	0.71871	1.3663	1	

Table 13 Case IV

$b=d$	c	$\tilde{\eta}_{\max}$	$\tilde{u}_{\max}$	$\tilde{c}_s$	$\rightarrow$	$\leftarrow$
$0.\overline{24}$	$-0.\overline{15}$	1.000000	0.866025	1.44337	1	
$0.\overline{26}$	$-0.\overline{16}$	0.97827	0.84893	1.4345	1	
0.2	−0.3	1.08642	1.02660	1.5149	2	
0.3	−0.5	1.00528	0.97966	1.4902	1+	

IV. Perturbation of the System Coefficients b, c, d

Initial conditions:

$$\begin{aligned} \eta_0(x) &= \eta_0 \operatorname{sech}^2\big(\lambda(x+x_0)\big), \\ u_0(x) &= B\eta_0 \operatorname{sech}^2\big(\lambda(x+x_0)\big), \end{aligned} \tag{5.4}$$

where $x_0 = 100$ and η_0, B, λ are the coefficients corresponding to $\theta^2 = 9/11$, i.e. as in Case I. Now we perturb the coefficients b, c, d of the system by a small amount so that the perturbed system is no longer a member of the Bona–Smith family, but so that there still holds $a = 0$, $b = d > 0$, and $c < 0$ and, therefore, the associated initial-value problem is well-posed. Note that for $\theta^2 = 9/11$, the original (unperturbed) Bona–Smith system has coefficients $a = 0$, $b = d = 8/33 = 0.\overline{24}$, $c = -5/33 = -0.\overline{15}$.

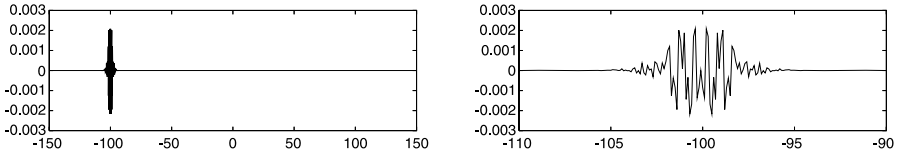

Fig. 20 The graph of $p(x; 10^5)$. (The plot on the right is a magnification of the one on the left)

Table 14 Case V

m	$\tilde{\eta}_{\max}$	$\tilde{u}_{\max}$	$\tilde{c}_s$	$\rightarrow$	$\leftarrow$
10^5	0.99994	0.86598	1.4433	1	0
10^7	1.05820	0.90937	1.4662	1	0

V. Numerical Noise in the Initial Condition of η

Bona–Smith system, $\theta^2 = 9/11$. Initial conditions:

$$\begin{aligned} \eta_0(x) &= \eta_0 \operatorname{sech}^2\big(\lambda(x + x_0)\big) + p(x; m), \\ u_0(x) &= B\eta_0 \operatorname{sech}^2\big(\lambda(x + x_0)\big), \end{aligned} \tag{5.5}$$

where x_0, η_0, B, λ as in Case I and where p is a "numerical" noise function defined as

$$p(x; m) = \big(\text{double}\big(\eta_s(x, 0)\big) - \text{single}\big(\eta_s(x, 0)\big)\big) \cdot m,$$

where $\eta_s(x, 0) = \eta_0 \operatorname{sech}^2(\lambda(x + x_0))$, $\text{double}(\eta_s(x, 0))$ is the double precision function $\eta_s(x, 0)$, and $\text{single}(\eta_s(x, 0))$ is the single precision function $\eta_s(x, 0)$. If $m = 10^7$, p is of the order of 10^{-1}, while if $m = 10^5$, p is of the order of 10^{-3}. The graph of $p(x; 10^5)$ is shown in Fig. 20 and the parameters of the emerging solitary waves in Table 14.

VI. Nonsymmetric Perturbations

Bona–Smith system, $\theta^2 = 9/11$.

(a) *Nonsymmetric perturbations of* η_0. Initial conditions:

$$\begin{aligned} \eta_0(x) &= \eta_0 \operatorname{sech}^2\big(\lambda(x + x_0)\big)\big(1 + \mu \tanh\big(0.5(x + x_0)\big)\big), \\ u_0(x) &= B\eta_0 \operatorname{sech}^2\big(\lambda(x + x_0)\big), \end{aligned} \tag{5.6a}$$

where x_0, η_0, B, and λ as in Case I.

(b) *Nonsymmetric perturbations of* $u_0(x)$. Initial conditions:

$$\begin{aligned} \eta_0(x) &= \eta_0 \operatorname{sech}^2\big(\lambda(x + x_0)\big), \\ u_0(x) &= B\eta_0 \operatorname{sech}^2\big(\lambda(x + x_0)\big)\big(1 + \mu \tanh\big(0.5(x + x_0)\big)\big), \end{aligned} \tag{5.6b}$$

where x_0, η_0, B, and λ as above.

Table 15 Case VI(a)

μ	$\tilde{\eta}_{\max}$	$\tilde{u}_{\max}$	$\tilde{c}_s$	$\rightarrow$	$\leftarrow$
0.1	1.00023	0.86620	1.4435	1	0
2	1.08541	0.92943	1.4768	1	0+
6	1.55470	1.25565	1.6507	1	1
6.25	1.58964	1.27898	1.6631	1	1
6.28	blow-up	blow-up			

Table 16 Case VI(b)

μ	$\tilde{\eta}_{\max}$	$\tilde{u}_{\max}$	$\tilde{c}_s$	$\rightarrow$	$\leftarrow$
8	1.91648	1.48539	1.7753	1	1
8.4	1.98656	1.52772	1.7985	1	1
8.5	blow-up	blow-up			

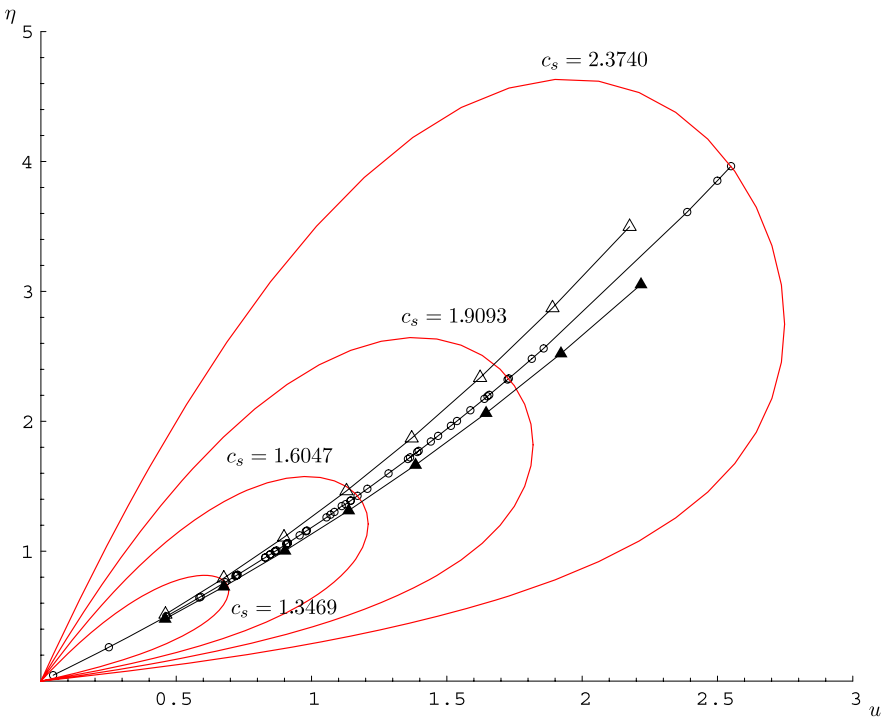

Fig. 21 ▲ ($\theta^2 = 1$), ∘ ($\theta^2 = 9/11$), △ ($\theta^2 = 2/3$)

Appendix 3: A Library of Solitary Waves

Figure 21 shows a collection of points in the first quadrant of the u, η-plane representing peak values $(u_{\max}, \eta_{\max})$ of solitary waves that we computed in our experiments for three systems of the Bona–Smith family, namely the "classical" Bona–

Smith system ($\theta^2 = 1$), the system that we often used in the numerical experiments ($\theta^2 = 9/11$), and the BBM–BBM system ($\theta^2 = 2/3$). Also shown are four indicative isospeed graphs of the equation $f(u, \eta) = 0$, see (1.13), in the first quadrant corresponding to four values of c_s. The (*straight*) line segments connecting the peak points for each system are not solitary-wave orbits but are just intended to serve as graphical approximations of the parametric dependence of the peaks $(u_{\max}, \eta_{\max})$ on c_s for the three systems. The figure suggests that for each value of θ^2, i.e. for each particular member of the Bona–Smith family, the peak $(u_{\max}, \eta_{\max})$ is a univalent, smooth function of c_s. (The peaks $u_{\max}$ and $\eta_{\max}$ increase with c_s, as we have seen.)

Acknowledgements The work of Dougalis and Mitsotakis was supported by a Pythagoras grant to the University of Athens co-funded by the Greek Ministry of Education and the E.U. European Social Fund. Travel and interaction between the Greek and the Spanish team was also supported by a Greece–Spain R&D Collaboration grant funded jointly by the General Secreteriat of Research and Technology, Greece, and the Ministry of Education and Science, Spain. López–Marcos was also supported by grant DGICYT MTM-2005-01739 and a grant by Junta de Castilla y León and the E.U. (FSE) VA 063/04. The authors wish to thank the University of Valladolid, and the Institute of Applied and Computational Mathematics of F.O.R.T.H. for their hospitality.

References

1. J. P. Albert, J. L. Bona, and D. Henry. Sufficient conditions for stability of solitary-wave solutions of model equations for long waves. *Physica D*, **24**:343–366, 1987.
2. D. C. Antonopoulos. The Boussinesq system of equations: Theory and numerical analysis. Ph.D. thesis. University of Athens, 2000 (in Greek).
3. D. C. Antonopoulos and V. A. Dougalis. Numerical approximation of Boussinesq systems. In A. Bermudez et al., editors, *Proceedings of the 5th International Conference on Mathematical and Numerical Aspects of Wave Propagation*, pages 265–269. SIAM, Philadelphia, 2000.
4. D. C. Antonopoulos, V. A. Dougalis, and D. E. Mitsotakis. Theory and numerical analysis of the Bona–Smith type systems of Boussinesq equations (to appear).
5. T. B. Benjamin. The stability of solitary waves. *Proc. R. Soc. Lond. Ser. A*, **328**:153–183, 1972.
6. J. L. Bona. On the stability theory of solitary waves. *Proc. R. Soc. Lond. Ser. A*, **344**:363–374, 1975.
7. J. L. Bona and M. Chen. A Boussinesq system for two-way propagation of nonlinear dispersive waves. *Physica D*, **116**:191–224, 1998.
8. J. L. Bona, M. Chen, and J.-C. Saut. Boussinesq equations and other systems for small-amplitude long waves in nonlinear dispersive media: I. Derivation and linear theory. *J. Nonlinear Sci.*, **12**:283–318, 2002.
9. J. L. Bona, M. Chen, and J.-C. Saut. Boussinesq equations and other systems for small-amplitude long waves in nonlinear dispersive media: II. The nonlinear theory. *Nonlinearity*, **17**:925–952, 2004.
10. J. L. Bona, V. A. Dougalis, O. A. Karakashian, and W. R. McKinney. Conservative, high-order numerical schemes for the generalized Korteweg–de Vries equation. *Philos. Trans. R. Soc. Lond. Ser. A*, **351**:107–164, 1995.
11. J. L. Bona, W. R. McKinney, and J. M. Restrepo. Unstable solitary-wave solutions of the generalized regularized long-wave equation. *J. Nonlinear Sci.*, **10**:603–638, 2000.
12. J. L. Bona and R. L. Sachs. The existence of internal solitary waves in a two-fluid system near the KdV limit. *Geophys. Astrophys. Fluid Dyn.*, **48**:25–51, 2000.
13. J. L. Bona and R. Smith. A model for the two-way propagation of water waves in a channel. *Math. Proc. Camb. Philos. Soc.*, **79**:167–182, 1976.
14. J. L. Bona, P. E. Souganidis, and W. A. Strauss. Stability and instability of solitary waves of KdV type. *Proc. R. Soc. Lond. Ser. A*, **411**:395–412, 1987.
15. J. V. Boussinesq. Théorie des ondes et des remous qui se propagent le long d' un canal rectangulaire horizontal, en communiquant au liquide contenu dans ce canal des vitesses sensiblement pareilles de la surface au fond. *J. Math. Pure Appl.*, **17**:55–108, 1872.

16. J. V. Boussinesq. Essai sur la théorie des eaux courants. *Mém. prés. div. sav. Acad. des Sci. Inst. Fr. (sér. 2)*, **23**:1–680, 1877.
17. M. Chen. Exact traveling-wave solutions to bi-directional wave equations. *Int. J. Theor. Phys.*, **37**:1547–1567, 1998.
18. M. Chen. Solitary-wave and multipulsed traveling-wave solutions of Boussinesq systems. *Appl. Anal.*, **75**:213–240, 2000.
19. V. A. Dougalis and D. E. Mitsotakis. Solitary waves of the Bona–Smith system. In D. Fotiadis and C. Massalas, editors, *Advances in Scattering Theory and Biomedical Engineering*, pages 286–294. World Scientific, River Edge, 2004.
20. A. Durán and M. A. López-Marcos. Conservative numerical methods for solitary wave interactions. *J. Phys. A: Math. Gen.*, **36**:7761–7770, 2003.
21. K. El Dika. Asymptotic stability of solitary waves for the Benjamin–Bona–Mahony equation. *Discrete. Contin. Dyn. Syst.*, **13**:583–622, 2005.
22. M. Grillakis, J. Shatah, and W. A. Strauss. Stability of solitary waves in the presence of symmetry: I. *J. Funct. Anal.*, **74**:170–197, 1987.
23. T. Kato. *Perturbation Theory for Linear Operators*, 2nd edn. Springer, Berlin, 1980.
24. Yi A. Li. Hamiltonian structure and linear stability of solitary waves of the Green–Naghdi equation. *J. Nonlinear Math. Phys.*, **9**:99–105, 2002. Suppl. I.
25. Y. Martel and F. Merle. Asymptotic stability of solitons for subcritical generalized KdV equations. *Arch. Rat. Mech. Anal.*, **157**:219–254, 2001.
26. J. R. Miller and M. I. Weinstein. Asymptotic stability of solitary waves for the Regularized Long-Wave equation. *Commun. Pure Appl. Math.*, **49**:399–441, 1996.
27. R. L. Pego, P. Smereka, and M. I. Weinstein. Oscillatory instability of solitary waves in a continuum model of lattice vibrations. *Nonlinearity*, **8**:921–941, 1995.
28. R. L. Pego and M. I. Weinstein. Asymptotic stability of solitary waves. *Commun. Math. Phys.*, **164**:305–349, 1994.
29. R. L. Pego and M. I. Weinstein. Convective linear stability of solitary waves for Boussinesq equations. *Stud. Appl. Math.*, **99**:311–375, 1997.
30. B. Pelloni. Spectral methods for the numerical solution of nonlinear dispersive wave equations. Ph.D. thesis, Yale University, 1996.
31. B. Pelloni and V. A. Dougalis. Numerical modelling of two-way propagation of nonlinear dispersive waves. *Math. Comput. Simul.*, **55**:595–606, 2001.
32. B. Pelloni and V. A. Dougalis. Numerical solutions of some nonlocal, nonlinear, dispersive wave equations. *J. Nonlin. Sci.*, **10**:1–22, 2000.
33. D. H. Peregrine. Equations for water waves and the approximations behind them. In R. E. Meyer, editor, *Waves on Beaches and Resulting Sediment Transport*, pages 95–121. Academic Press, New York, 1972.
34. M. Reed and B. Simon. *Analysis of Operators IV*. Academic Press, New York, 1978.
35. P. C. Schuur. *Asymptotic Analysis of Soliton Problems: An Inverse Scattering Approach*, volume 1232 of *Lecture Notes in Mathematics*. Springer, Berlin, 1986.
36. P. Smereka. A remark on the solitary wave stability for a Boussinesq equation. In L. Debnath, editor, *Nonlinear Dispersive Wave Systems*, pages 255–263. World Scientific, Singapore, 1992.
37. J. F. Toland. Solitary wave solutions for a model of the two-way propagation of water waves in a channel. *Math. Proc. Camb. Philos. Soc.*, **90**:343–360, 1981.
38. J. F. Toland. Uniqueness and a priori bounds for certain homoclinic orbits of a Boussinesq system modelling solitary water waves. *Commun. Math. Phys.*, **94**:239–254, 1984.
39. J. F. Toland: Existence of symmetric homoclinic orbits for systems of Euler–Lagrange equations. In *Proceedings of Symposia in Pure Mathematics*, volume 45, Part 2, pages 447–459. Am. Math. Soc., Providence, 1986.
40. M. Weinstein. Lyapunov stability of ground states of nonlinear dispersive evolution equations. *Commun. Pure Appl. Math.*, **39**:51–68, 1986.
41. M. Weinstein. Existence and dynamic stability of solitary-wave solutions of equations arising in long wave propagation. *Commun. Partial Differ. Eq.*, **12**:1133–1173, 1987.
42. M. I. Weinstein. Asymptotic stability of nonlinear bound states in conservative dispersive systems. *Contemp. Math.*, **200**:223–235, 1996.
43. G. B. Whitham. *Linear and Non-linear Waves*. Wiley, New York, 1974.
44. R. Winther. A finite element method for a version of the Boussinesq equations. *SIAM J. Numer. Anal.*, **19**:561–570, 1982.
45. N. J. Zabusky and M. D. Kruskal. Interaction of "solitons" in a collisionless plasma and the recurrence of initial states. *Phys. Rev. Lett.*, **15**:240–243, 1965.